# *Ab Initio* Path-Integral Calculations of Kinetic and Equilibrium Isotope Effects on Base-Catalyzed RNA Transphosphorylation Models

Kin-Yiu Wong,*[a,b] Yuqing Xu,[a,b] and Darrin M. York*[c]

Detailed understandings of the reaction mechanisms of RNA catalysis in various environments can have profound importance for many applications, ranging from the design of new biotechnologies to the unraveling of the evolutionary origin of life. An integral step in the nucleolytic RNA catalysis is self-cleavage of RNA strands by 2′-*O*-transphosphorylation. Key to elucidating a reaction mechanism is determining the molecular structure and bonding characteristics of transition state. A direct and powerful probe of transition state is measuring isotope effects on biochemical reactions, particularly if we can reproduce isotope effect values from quantum calculations. This article significantly extends the scope of our previous joint experimental and theoretical work in examining isotope effects on enzymatic and nonenzymatic 2′-*O*-transphosphorylation reaction models that mimic reactions catalyzed by RNA enzymes (ribozymes), and protein enzymes such as ribonuclease A (RNase A). Native reactions are studied, as well as reactions with thio substitutions representing chemical modifications often used in experiments to probe mechanism. Here, we report and compare results from eight levels of electronic-structure calculations for constructing the potential energy surfaces in kinetic and equilibrium isotope effects (KIE and EIE) computations, including a "gold-standard" coupled-cluster level of theory [CCSD(T)]. In addition to the widely used Bigeleisen equation for estimating KIE and EIE values, internuclear anharmonicity and quantum tunneling effects were also computed using our recently developed *ab initio* path-integral method, that is, automated integration-free path-integral method. The results of this work establish an important set of benchmarks that serve to guide calculations of KIE and EIE for RNA catalysis. © 2014 Wiley Periodicals, Inc.

**DOI: 10.1002/jcc.23628**

## Introduction

Elucidation of RNA catalytic mechanisms has a wide range of implications and applications, from the evolutionary origin of life and cell signaling to the design of new biotechnologies and therapeutics.[1–7] Of particular importance, are the nucleolytic RNA enzymes (ribozymes) that catalyzes a 2′-*O*-transphosphorylation for the self-cleavage processes of RNA strands.[1–17] Every potential reaction path associated with the 2′-*O*-transphosphorylation is characterized by its own rate-limiting transition state, which, by its nature (in contrast to reactant and product states), is unstable and thus is very hard to be captured in experiment (it is also generally true for other types of biochemical reactions as well). As a result, determining the molecular structure and bonding of the rate-limiting transition state with the aid of the computers is a key component in unraveling the catalytic mechanisms of these ribozymes.[8–11,18–29]

To shed some light on the nature of the transition-state structure and bonding, studying equilibrium and kinetic isotope effects (EIE and KIE) on a biochemical reaction is a popular and powerful approach.[8,9,18–22,26–29] The EIE is defined as the ratio of equilibrium constant of light isotope to that of heavy isotope:

$$\mathrm{EIE} \equiv \frac{\text{Equilibrium constant (light isotope)}}{\text{Equilibrium constant (heavy isotope)}} \tag{1}$$

And the KIE is defined as the ratio of reaction rate of light isotope to that of heavy isotope:

$$\mathrm{KIE} \equiv \frac{\text{Rate (light isotope)}}{\text{Rate (heavy isotope)}} \tag{2}$$

If KIE value is larger than unity, then we call it as "normal KIE" because the reaction rate of light isotope is faster than that of heavy isotope. On the contrary, an "inverse KIE" means that the KIE value is smaller than unity, that is, the reaction

[a] *K.-Y. Wong, Y. Xu*
*Department of Physics, High Performance Cluster Computing Centre, Institute of Computational and Theoretical Studies, Hong Kong Baptist University, 224 Waterloo Road, Kowloon Tong, Hong Kong*
*E-mail (K.-Y. Wong): wongky@hkbu.edu.hk, kiniu@alumni.cuhk.net*
[b] *K.-Y. Wong, Y. Xu*
*Institute of Research and Continuing Education, Hong Kong Baptist University (Shenzhen), Shenzhen, China*
[c] *D. M. York*
*Department of Chemistry & Chemical Biology, Center for Integrative Proteomics Research, BioMaPS Institute for Quantitative Biology, Rutgers, The State University of New Jersey, 174 Frelinghuysen Road, Piscataway, New Jersey 08854*
*E-mail: york@biomaps.rutgers.edu*
Contract grant sponsor: US NIH (D.M.Y.); Contract grant number: GM064288; Contract grant sponsor: HK RGC (K.-Y.W); Contract grant number: ECS-209813; Contract grant sponsor: NSF of China; Contract grant number: NSFC-21303151; Contract grant sponsor: HKBU FRG; Contract grant number: FRG2/12-13/037; Contract grant sponsor: HKBU startup funds; Contract grant number: 38-40-088 and 40-49-495; Contract grant sponsor: National Science Foundation [Extreme Science and Engineering Discovery Environment (XSEDE), with project number TG-MCB110101 (D.M.Y.)]; Contract grant number: OCI-1053575

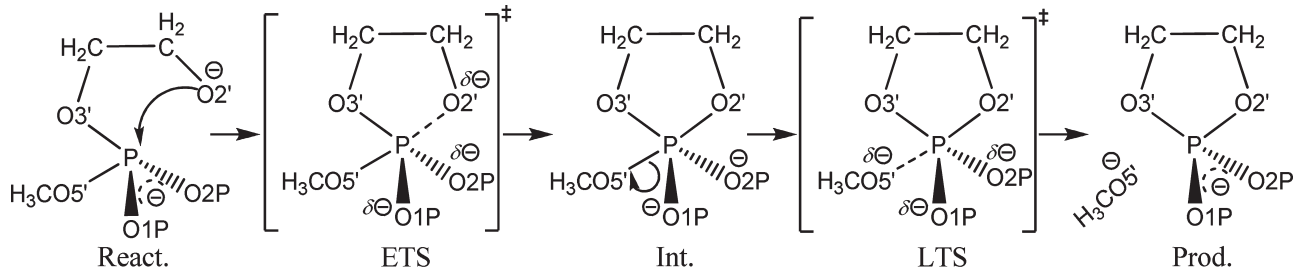


**Scheme 1.** General reaction scheme for the (associative) reverse of dianionic in-line methanolysis of ethylene phosphate: a model for RNA phosphate transesterification under alkaline conditions. "React.," "ETS," "Int.," "LTS," and "Prod." stand for reactant, early transition state, intermediate, late transition state, and product, respectively. In the present work, the native reaction in the scheme is studied in both gas and solution phases as well as reactions that have single sulfur substitutions in the bridging 3′- (S3′) and leaving group 5′-positions (S5′). Note: as revealed by our calculations, not all of the states in the scheme exist for every reaction (see text for details).

rate of light isotope is slower than that of heavy isotope. This reaction rate ratio, that is, KIE, is very sensitive to the rate-limiting transition state. Therefore, measuring KIE values has been considered as a (most) direct and powerful experimental probe of transition state.[8,9,18–22,26–29] Furthermore, for some cases of 2′-*O*-transphosphorylation, the O2′ position may or may not be deprotonated in a preequilibrium step. Hence, it is also important to study the EIE on the 2′-OH deprotonation as well.[8,9,30]

Nevertheless, such important experimental numerical values of KIE cannot directly tell us what the structure of the rate-limiting transition state precisely is. As a result, isotope effects computation and computational visualization provide us with a complementary approach for identifying the structure of the rate-limiting transition state.

This is because, in contrast to experiment, prior to calculating the numerical values of isotope effects, we first hypothesize a reaction path to determine an explicit molecular structure of the rate-limiting transition state.[8–11,18–29] Subsequently, we would like to validate whether or not our computed isotope-effect values associated with the hypothetical transition-state structure match with experimental results. If so, then we can safely conclude that the enzymatic mechanism, along with the molecular structure, bonding, and other properties of the rate-limiting transition state, are successfully determined *in silico* that otherwise can only be qualitatively inferred.[8,9,18–22,26–29]

Indeed, previously, a collaborative computational and experimental investigation has been coordinated to study the isotope effects on the base-catalyzed RNA transphosphorylation. As demonstrated in our previous communication,[9] a simplest model for studying the essence of the transphosphorylation is the reverse, dianionic, in-line methanolysis of ethylene phosphate. The general mechanism of the methanolysis is shown
S1 in Scheme 1, in which the phosphoryl oxygen positions are labeled in accordance with their RNA counterparts.

In that communication,[9] the free-energy profile[31,32] for the reaction mechanism illustrated in Scheme 1 was generated via molecular dynamics simulations[33] using potential energy constructed on the fly by density-functional quantum mechanical/molecular mechanical (QM/MM) approach in explicit solvent.[31] These high-level and expensive free-energy simulations were performed with a modified version of the CHARMM program (based on c36a2 version),[34] interfacing with the Q-Chem program.[35] As a result, the dynamic fluctuations of the solute and the degrees of freedom of the water molecules are all incorporated. In addition, the adiabatic energy profile was also determined by implicit solvent of the polarizable continuum model (PCM).[36–41] The levels of density-functional theory (DFT)[42,43] for both profiles in explicit and implicit solvation models are the same, which are the hybrid B3LYP[44] exchange-correlation functional with the 6-31+G(d) basis set.[45,46] We have concluded that the DFT QM/MM free-energy profile and the PCM adiabatic energy profile are quite similar.[9] Both are in an associative mechanism and possess early and late transition states (ETS and LTS). Both LTS are the rate-limiting transition states, with 24.1 and 21.0 kcal/mol barriers, respectively.[9] The calculated PCM barrier (21.0 kcal/mol) is close to the experimental derived rate for UpG phosphate transesterification (19.9 kcal/mol), extrapolated at the infinite pH limit.[9] Moreover, the calculated and experimental KIE values are also in good agreement, in particular our calculations clearly indicate that the rate-limiting transition state is shifted from LTS to ETS with thio substitution at either 3′ or 5′ position. All these results suggest that our PCM calculations are able to describe the core of the solvent effects on the energy profile for computing the KIE and EIE values.

Subsequently, another coordinated work of experiment and theory about isotope effects was just published for determining the altered transition-state structures of the 2′-*O*-transphosphorylation catalyzed by ribonuclease A (RNase A).[8]

By virtue of all these successful stories about the computations on isotope effects on the 2′-*O*-transphosphorylation, there has been a definite need for a detailed comparative study on the accuracy, robustness, and computing time at various levels of electronic-structure and internuclear quantum theories. As a result, in this article, KIE and EIE calculations on the base-catalyzed RNA transphosphorylation in both gas and solution phases at a total of eight different levels of electronic-structure theory are reported. These eight levels of theory for constructing the potential energy surfaces range from the single-Slater-determinant Hartree–Fock method (HF)[45,46] and two popular DFT approaches,[42–44,47,48] to the multi-Slater-determinant Møller-Plesset (MP) perturbation method,[45,49] single-and-double-

substitution coupled-cluster (CCSD) theory, and a "gold-standard" partial-triple-substitution coupled-cluster [CCSD(T)] theory.[45,50,51] And the three basis sets that were tested are 3-21+G*, 6-31+G(d), and 6-311+G(d,p).[45,46] Furthermore, internuclear quantum-statistical effects were taken care by the conventional Bigeleisen equation[8,9,22,52,53] as well as by our recently developed automated integration-free path-integral (AIF-PI) method for calculating anharmonicity and quantum tunneling effects.[9,22,31,54–56] We hope our benchmark reported herein can establish a mini database serving a guide for future more accurate and more efficient isotope-effect computations and free-energy simulations on more complex biomolecular systems of RNA catalysis.

## Computational Details

17 and 16 nuclei are in anionic and dianionic reactions, respectively, for which 82 electrons are in each native reactant and in each native transition state, while 90 electrons are in each thio-substituted reactant and in each thio-substituted transition state. The molecular structures of the native and thio-substituted anionic and dianionic reactants, and the transition-state structures were minimized in the gas phase and in aqueous solution using HF theory,[45,46] second-order MP perturbation method (MP2),[45,49] and DFT methods,[42–44,47,48] with the inclusion of the PCM[36–41] for treating the solvent effects. Two popular hybrid-exchange-correlation density-functionals, B3LYP[44] and M06-2X,[47,48] were employed. The three different basis sets we used in this work are among those most frequently used in biomolecular applications: 3-21+G*, 6-31+G(d), and 6-311+G(d,p).[45,46] Coupled-cluster single-point energy calculations at the levels of CCSD/6-311+G(d,p) and "gold-standard" CCSD(T)/6-311+G(d,p)[45,50,51] were performed on each of the minimized structures in both gas and solution phases. Vibrational frequency analyses were carried out to confirm the nature of the minimum and saddle points, and to compute quantum thermal corrections in the decoupled rigid-rotor harmonic-oscillator approximation.[57] The software package Gaussian 09 was used for all the electronic-structure calculations.[41]

An essential feature of Gaussian 09 that enables these calculations to be performed was the implementation of a continuous surface charge formalism based on a smooth boundary element solvation method that afforded continuity, smoothness, and robustness of the solvent reaction field and its derivatives with respect to nuclear positions.[36–41] We have used the UAKS radii optimized at the PB0/6-31G(d) level of theory[57,58] to define the molecular cavity for the PCM model,[58,59] with special tuning of the radii at the 2′-OH and X5′ positions, so as to be fixed along the reaction coordinate and close to the QM/MM and experimental barrier values. All fixed atomic radii used in the present work (which can ensure the continuity of the PCM energy surface), and the gas-phase and solution-phase minimized structures are given in Supporting Information.

The most widely used formalism to compute EIE and KIE is the Bigeleisen equations[8,9,22,52,53] (fulfilling the Redlich–Teller product rule[52,53]), in which the EIE and KIE are evaluated in terms of harmonic vibrational frequencies, and neglecting quantum tunneling:

$$\mathrm{EIE_{BE}} = \frac{\prod_{i=1}^{3N-6} \frac{\Omega^P_{i,l_0}/\sinh(\beta\hbar\Omega^P_{i,l_0}/2)}{\Omega^P_{i,h_0}/\sinh(\beta\hbar\Omega^P_{i,h_0}/2)}}{\prod_{i=1}^{3N-6} \frac{\Omega^R_{i,l_0}/\sinh(\beta\hbar\Omega^R_{i,l_0}/2)}{\Omega^R_{i,h_0}/\sinh(\beta\hbar\Omega^R_{i,h_0}/2)}} \tag{3}$$

$$\mathrm{KIE_{BE}} = \left(\frac{\omega^\ddagger_{l_0}}{\omega^\ddagger_{h_0}}\right) \frac{\prod_{i=1}^{3N-7} \frac{\Omega^\ddagger_{i,l_0}/\sinh(\beta\hbar\Omega^\ddagger_{i,l_0}/2)}{\Omega^\ddagger_{i,h_0}/\sinh(\beta\hbar\Omega^\ddagger_{i,h_0}/2)}}{\prod_{i=1}^{3N-6} \frac{\Omega^R_{i,l_0}/\sinh(\beta\hbar\Omega^R_{i,l_0}/2)}{\Omega^R_{i,h_0}/\sinh(\beta\hbar\Omega^R_{i,h_0}/2)}} \tag{4}$$

where $\hbar$ is Planck's constant divided by $2\pi$, $\beta = 1/k_BT$, $k_B$ is Boltzmann's constant, $T$ is absolute temperature, the superscripts ‡, $P$, and $R$ denote the transition state, product state, and reactant state, respectively, $\omega^\ddagger$ is the imaginary frequency at the transition state, $l_0$ indicates the light isotope and $h_0$ is the heavy isotope, $N$ is the number of nuclei, $i$ is the index running over all normal modes, and $\Omega_i$ is the real frequency for the $i$th normal mode.

To go beyond the harmonic approximation and to include quantum tunneling effects in the framework of the Feynman centroid path integral (PI), we refine the Bigeleisen equations as follows:[9,22,60]

$$\mathrm{EIE_{PI}} = \frac{\exp[-\beta(W^P_{l_0} - W^P_{h_0})]}{\exp[-\beta(W^R_{l_0} - W^R_{h_0})]} \tag{5}$$

$$\mathrm{KIE_{PI}} = \left(\frac{\omega^\ddagger_{l_0}}{\omega^\ddagger_{h_0}}\right) \frac{\exp[-\beta(W^\ddagger_{l_0} - W^\ddagger_{h_0})]}{\exp[-\beta(W^R_{l_0} - W^R_{h_0})]} \tag{6}$$

where $W$ is the centroid effective potential energy calculated at the centroid position of path integrals.[31,54,61–69] The mass (isotope)- and temperature-dependent nature of the centroid potential energy $W$ distinguishes itself from the (*ab initio*) Born–Oppenheimer potential energy. The latter is independent of temperature and (nuclear) mass. Note that our refined Bigeleisen equations, that is, Eqs. (5) and (6), reduce back to the well-known Bigeleisen equations [i.e., Eqs. (3) and (4)] when the centroid potential is computed in the decoupled rigid-rotor harmonic-oscillator approximation (and neglecting tunneling effects; Appendix B in Ref. [60] provides a proof). In addition, Eqs. (5) and (6) are consistent with the PI transition-state theory (PI-QTST),[65,67,70–72] and the reaction coordinate is defined as the centroid positions of path integrals of nuclear configurations, which are the imaginary time-average positions of nuclei. The mass-dependent property of the centroid potential in the formulation of the PI-QTST has already been applied to chemical reactions in condensed phases.[63–67,70,73–81]

In this work, with the treatment of solvent effects by a dielectric continuum, we used our AIF-PI method[31,54–56] to determine the values of $W$, and then in turn used Eqs. (5) and (6) to compute EIE and KIE values along the reaction path of intrinsic reaction coordinate (IRC) on the *ab initio* potential energy surface.[9,22] Our AIF-PI method is based on the powerful and remarkably accurate Kleinert's variational perturbation

**Table 1.** Computing times of single-point energy, force, and frequency calculations at the eight levels of electronic structure theory.[a]

| Native LTS in solution: Electronic Structure Theory | Four processors, 4-GB memory, computing time (hh:mm:ss)[b] | | |
|---|---|---|---|
| | Energy | Force | Frequency |
| HF/3-21+G* | 00:00:09 | 00:00:13 | 00:01:07 |
| B3LYP/6-31+G(d) | 00:00:34 | 00:00:42 | 00:04:35 |
| M06-2X/6-31+G(d) | 00:00:48 | 00:00:57 | 00:06:32 |
| B3LYP/6-311+G(d,p) | 00:01:17 | 00:01:34 | 00:11:25 |
| M06-2X/6-311+G(d,p) | 00:01:26 | 00:01:45 | 00:17:35 |
| MP2/6-311+G(d,p) | 00:01:19 | 00:04:04 | 02:10:38 |
| CCSD/6-311+G(d,p) | 01:51:14 | _[c] | _[c] |
| CCSD(T)/6-311+G(d,p) | 04:54:00 | _[c] | _[c] |

[a] The number of basis functions in this table for 3-21+G*, 6-31+G(d), and 6-311+G(d,p) are 141, 189, and 248, respectively. All calculations were performed with four processors of Intel Xeon E7-4870 2.40 GHz, sharing 4-GB memory of 1066 MHz quad ranked LV RDIMMs, on a single-compute-node machine (jiraiya) that has 40 processors of Intel Xeon E7-4870 2.40GHz (4×10C), sharing 1 TB memory of 1066 MHz quad ranked LV RDIMMs (64×16GB). The LTS structures are the optimized structures in solution, respectively, for each level of theory, except for CCSD and CCSD(T) single-point energy calculations. In these CCSD and CCSD(T) calculations, we used the optimized structure in solution at the MP2/6-311+G(d,p) level. [b] hh = hours in two digits, mm = minutes in two digits, ss = seconds in two digits. [c] The calculation was not performed by us.

(KP) theory [which has been shown accurate even at the limit of zero temperature (absolute zero) and at the electronic scale],[61,82–87] and makes use of the decoupled instantaneous normal coordinate approximation (DINCA) to render the KP theory be applicable to actual molecular systems.[31,54–56,88] Our previous studies on a series of proton-transfer reactions demonstrate that performing *ab initio* PI calculations with our AIF-PI method can accurately and economically include anharmonicity and tunneling contributions to the KIE values calculated from Eq. (6). These two contributions are important to have quantitative agreement with experimental results.[22] Furthermore, we also have successfully used our AIF-PI method to compute KIE on heavy nuclei.[9] Since the molecular structures at the stationary points of the original gas-phase and solution-phase Born–Oppenheimer potential energy surfaces (PES) should be similar to those on the gas-phase and solution-phase centroid PES (their difference is usually in the order of magnitude of about 0.01 Å),[56] the molecular structures of the reactant and transition states were not reoptimized on the basis of the centroid potential.[9,22]

In the AIF-PI method, we interpolated the original gas-phase and solution-phase PES along each normal mode by a 20$^{th}$-order polynomial at a step size of 0.1 Å.[31,54–56] The centroid potential is computed up to the second order of KP expansion. Thus, the notation for this level of theory is KP2/P20, where P*m* denotes an *m*th-order polynomial representation of the original PES along each normal mode coordinate. Through a series of rigorous tests, we found that KP2/P20 is generally a good choice for the AIF-PI method. The calculated values of the centroid potential are usually within a few percent from the exact.[31,54–56]

In this work, the entire system is quantized (16 or 17 nuclei) to compute harmonic or Bigeleisen EIE and KIE values.

**Table 2.** Single-level relative free energy calculated for stationary points along the intrinsic reaction coordinate of the (A) native, (B) S3′, and (C) S5′ simplest models of RNA transphosphorylation in both gas and solution phases.[a]

| Electronic structure theory | Gas (kcal/mol) | | | Solution (kcal/mol) | | |
|---|---|---|---|---|---|---|
| | $\Delta G^{\ddagger}_{ETS}$ | $\Delta G_{Int}$ | $\Delta G^{\ddagger}_{LTS}$ | $\Delta G^{\ddagger}_{ETS}$ | $\Delta G_{Int}$ | $\Delta G^{\ddagger}_{LTS}$ |
| (A) Native (37°C) | | | | | | |
| HF/3-21+G* | – | – | 57.8 | 23.6 | 23.2 | 29.1 |
| B3LYP/6-31+G(d) | – | – | 41.3 | 18.6 | 18.3 | 21.0 |
| M06-2X/6-31+G(d) | – | – | 41.6 | 15.5 | 13.5 | 19.2 |
| B3LYP/6-311+G(d,p) | – | – | 41.1 | 18.5[b] | _[c] | 20.9 |
| M06-2X/6-311+G(d,p) | – | – | 42.2 | 15.2 | 13.9 | 19.4 |
| MP2/6-311+G(d,p) | – | – | 41.4 | 17.7 | 17.4 | 20.7 |
| (B) S3′ (37°C) | | | | | | |
| HF/3-21+G* | 40.8 | _[c] | 39.9 | 20.2 | 17.0 | 20.3 |
| B3LYP/6-31+G(d) | 34.6 | 34.0 | 35.5 | 16.9 | 16.0 | 17.8 |
| M06-2X/6-31+G(d) | 33.0 | 29.4 | 34.4 | 13.7 | 9.5 | 14.4 |
| B3LYP/6-311+G(d,p) | 33.8 | 33.5 | 34.7 | 16.3 | 15.9 | 17.2 |
| M06-2X/6-311+G(d,p) | 31.9 | 28.7 | 33.6 | 12.7[d] | 9.1[d] | 13.4[d] |
| MP2/6-311+G(d,p) | 32.4 | 31.4 | 33.2 | 15.8 | 14.0 | 16.4 |
| (C) S5′ (37°C) | | | | | | |
| HF/3-21+G* | 35.8 | – | – | 19.5 | – | – |
| B3LYP/6-31+G(d) | 26.6 | – | – | 16.6 | – | – |
| M06-2X/6-31+G(d) | 26.4 | – | – | 13.1 | – | – |
| B3LYP/6-311+G(d,p) | 25.9 | – | – | 16.4 | – | – |
| M06-2X/6-311+G(d,p) | 25.6 | – | – | 13.2 | – | – |
| MP2/6-311+G(d,p) | 27.0 | – | – | 15.7 | – | – |

[a] Thermal corrections of free energy are computed in the decoupled rigid-rotor harmonic-oscillator approximation. The PCM energy profiles shown in Figure 1 are shifted by thermal corrections at their respective rate-limiting transition states. "–" denotes the molecular structure of that particular state could not be determined by us. [b] The ETS is determined but along with very small value of non-reactive imaginary frequency. [c] No intermediate could be determined by us that satisfies all default criteria in GAUSSIAN 09.[41] [d] The reactant is determined but along with very small value of nonreactive imaginary frequency.

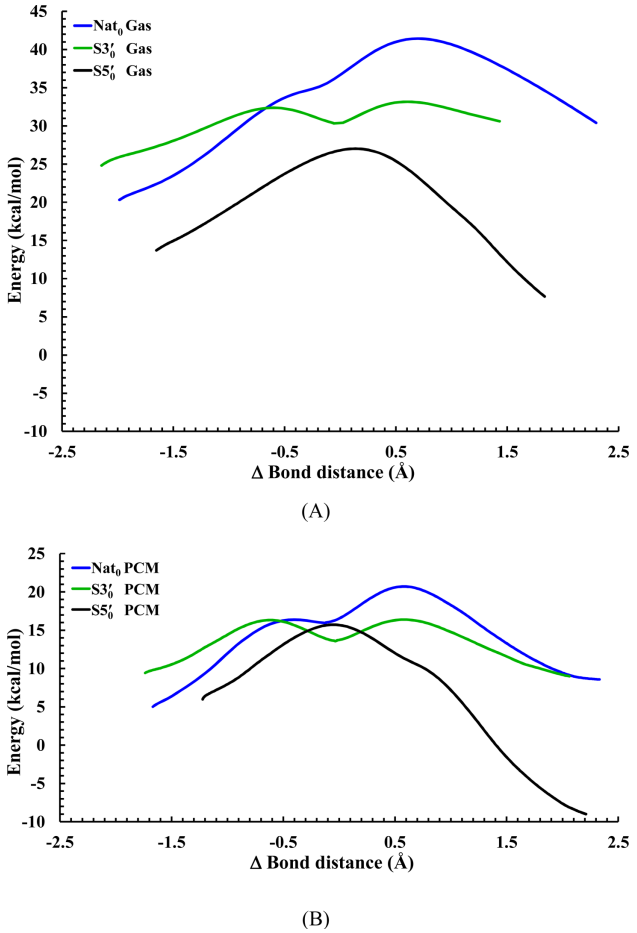


**Figure 1**. Adiabatic energy profiles for the native, S3′, and S5′ simplest models of RNA transphosphorylation in both (A) gas and (B) solution phases, as a function of the difference in bond length (Δbond) between the breaking P—X5′ bond (X = O for native and S3′; X = S for S5′) and the forming P—O2′ bond (Δbond = P—X5′ − P—O2′). The level of all the electronic structure calculations is at MP2/6-311+G(d,p). The profiles are mapped from the IRC paths and have been shifted to match the respective rate-limiting free-energy barriers calculated in the decoupled rigid-rotor harmonic-oscillator approximation at 37°C. Other than this shift, however, there is no zero-point energy or thermal corrections included in the profiles.

Additionally, for estimating the anharmonic and tunneling effect corrections to the Bigeleisen EIE and KIE values, we further quantize the following six to seven nuclei using the AIF-PI method: the phosphorus nucleus and all the five (oxygen or sulfur) nuclei that can potentially form covalent bonds to the phosphorus nucleus, including the O2′ of nucleophile and O5′/S5′ of leaving groups, in addition to the hydrogen nucleus connected with the O2′ (i.e., the H of 2′-OH) for the case of anionic ethylene phosphate bonded with methanol group. All our path integral calculations were performed using our AIF-PI program implemented for use with MATHEMATICA.[89]

## Results and Discussion

### Computational costs

Table 1 shows the computational costs of all eight levels of electronic structure theory, in terms of the computing times of single-point energy, force, and frequency calculations on the LTS structure of the native reaction in solution, using four processors and sharing 4-GB memory. HF/3-21+G* indeed is the computationally cheapest level of theory. DFT methods with the larger basis sets, 6-31+G(d) and 6-311+G(d,p), are obviously more computationally expensive, though are still affordable [e.g., the computing time for a frequency analysis at the level of M06-2X/6-311+G(d,p) is about 17 min].

Noteworthily, the computational cost for a single-point energy calculation at the MP2/6-311+G(d,p) level is virtually the same as those calculations at a DFT level using the same basis set. Nevertheless, the force and frequency analysis at the MP2 level are (significantly) more computationally expensive than the DFT methods, particularly true for the frequency analysis.

According to Table 1, CCSD is so computationally expensive that its single-point energy calculation took more or less the same amount of time as a frequency analysis at the MP2 level. The computational cost grows even much more terrifically for the "gold standard" CCSD(T) level of theory, as its single-point energy calculation took more than double of the computing time for a single-point energy calculation at the CCSD level (∼5 hours vs. ∼2 hours).

As shown in Table S1 (Supporting Information), similar conclusions as the above can be drawn when we increase the number of processors and the amount of the sharing memory from four to 16, and from 4 GB to 100 GB, respectively. One final remark is that the computing time for a single-point energy calculation at the CCSD(T) level using 16 processors is more or less the same as a frequency analysis at the MP2 level using four processors [Table S1 (Supporting Information)].

### Energetics

Table 2 lists the energy values for stationary points of the native and thio-substituted S3′ and S5′ reactions in both gas and solution phases, calculated at the six different levels of electronic structure theory. The corresponding energy profiles in both gas and solution phases at the MP2/6-311+G(d,p) level are shown in Figure 1. By comparing the results between gas and solution phases, it is clear that the solvation effects greatly reduce the rate-limiting barriers for all reactions. The extent of the reduction is most profound for the native reaction (by ∼20–30 kcal/mol), followed by the S3′ reaction (by ∼15–20 kcal/mol), and then the S5′ reaction (by ∼10–15 kcal/mol).

In the gas-phase native reaction, neither ETS nor intermediate (Scheme 1) could be determined at all six levels of theory. However, the polarization by the aqueous environment stabilizes the pentavalent phosphorane more than the LTS, which in turn induces a non-rate-limiting ETS and a transient intermediate in the solution-phase native reaction at all six levels of theory, except interestingly, no intermediate could be located by us at the B3LYP/6-311+G(d,p) level that satisfies all default criteria in GAUSSIAN 09.[41]

In contrast to the gas-phase native reaction, both ETS and metastable intermediate do exist in the gas-phase S3′ reaction at all six levels of theory, except interestingly, no intermediate could be located by us at the HF/3-21+G* level that satisfies

**Table 3.** Dual-level CCSD(T) relative free energy calculated for stationary points along the intrinsic reaction coordinate of the (A) native, (B) S3′, and (C) S5′ simplest models of RNA transphosphorylation in both gas and solution phases.[a]

| Electronic structure theory CCSD(T)/6-311+G(d,p) // | Gas (kcal/mol) | | | Solution (kcal/mol) | | |
|---|---|---|---|---|---|---|
| | $\Delta G^{\ddagger}_{ETS}$ | $\Delta G_{Int}$ | $\Delta G^{\ddagger}_{LTS}$ | $\Delta G^{\ddagger}_{ETS}$ | $\Delta G_{Int}$ | $\Delta G^{\ddagger}_{LTS}$ |
| (A) Native (37°C) | | | | | | |
| HF/3-21+G* | – | – | 40.8 | 17.5 | 17.5 | 20.2 |
| B3LYP/6-31+G(d) | – | – | 41.3 | 17.4 | 17.0 | 20.3 |
| M06-2X/6-31+G(d) | – | – | 41.0 | 17.1 | 17.3 | 20.1 |
| B3LYP/6-311+G(d,p) | – | – | 41.5 | 17.2[b] | _[c] | 20.2 |
| M06-2X/6-311+G(d,p) | – | – | 41.4 | 17.2 | 17.1 | 20.2 |
| MP2/6-311+G(d,p) | – | – | 41.1 | 17.6 | 17.5 | 20.5 |
| (B) S3′ (37°C) | | | | | | |
| HF/3-21+G* | 32.2 | _[c] | 33.5 | 16.0 | 14.7 | 16.2 |
| B3LYP/6-31+G(d) | 32.3 | 31.4 | 33.5 | 15.0 | 13.5 | 15.7 |
| M06-2X/6-31+G(d) | 32.8 | 32.6 | 33.5 | 14.9 | 13.6 | 15.1 |
| B3LYP/6-311+G(d,p) | 32.3 | 31.5 | 33.8 | 15.0 | 13.6 | 15.9 |
| M06-2X/6-311+G(d,p) | 32.2 | 32.0 | 33.2 | 14.4[d] | 13.1[d] | 14.7[d] |
| MP2/6-311+G(d,p) | 32.2 | 31.6 | 33.0 | 15.5 | 14.2 | 16.2 |
| (C) S5′ (37°C) | | | | | | |
| HF/3-21+G* | 25.9 | – | – | 15.6 | – | – |
| B3LYP/6-31+G(d) | 26.5 | – | – | 16.3 | – | – |
| M06-2X/6-31+G(d) | 27.1 | – | – | 15.5 | – | – |
| B3LYP/6-311+G(d,p) | 26.7 | – | – | 16.5 | – | – |
| M06-2X/6-311+G(d,p) | 26.7 | – | – | 15.8 | – | – |
| MP2/6-311+G(d,p) | 26.8 | – | – | 15.7 | – | – |

[a] CCSD(T) is not included in the thermal corrections. The thermal corrections are treated at their respective single-level calculations. See footnote [a] in Table 2 for details. "–" denotes the molecular structure of that particular state could not be determined by us. [b] As in Table 2, the ETS is determined but along with very small value of nonreactive imaginary frequency. [c] As in Table 2, no intermediate could be determined by us that satisfies all default criteria in Gaussian 09.[41] [d] As in Table 2, the reactant is determined but along with very small value of non-reactive imaginary frequency.

all default criteria in Gaussian 09.[41] For the S5′ reaction in both gas and solution phases, as opposed to both native and S3′ reactions, only ETS can be determined. There is no LTS, and thus no transient intermediate can be located at all six levels of theory.

In addition to these six levels of theory, we have also carried out computationally expensive single-point-energy coupled-cluster electronic-structure calculations, up to the "gold standard" CCSD(T)/6-311+G(d,p) level,[45,50,51] on the stationary points of these six levels of theory, that is, dual-level calculations. Results are presented in Table 3 for CCSD(T) and Table S2 (Supporting Information) for CCSD, in which all single-point CCSD(T) and CCSD energy calculations are only for electronic structure, and are not included in the nuclear thermal corrections. By comparing the results between Tables 2 and 3, it is evident that among those six single levels of theory, MP2/6-311+G(d,p) is the most accurate for our simplest models of RNA phosphate transesterification. This is because as shown in Table S3 (Supporting Information), the theory that exhibits the smallest root-mean-square deviation (RMSD) between its single-level calculations, and its counterpart of dual-level CCSD(T)/6-311+G(d,p) single-point energy calculations is MP2/6-311+G(d,p). This RMSD of MP2/6-311+G(d,p) is merely 0.2 kcal/mol (the largest deviation is just 0.3 kcal/mol). In other words, it should also be safely to interpret that among all single and dual levels of theory presented in this article (a total of 12 levels of theory), the most accurate calculations for our simplest models of RNA transphosphorylation are at the CCSD(T)/6-311+G(d,p)//MP2/6-311+G(d,p) dual level.

Yet, a very notable finding in this article is actually located by comparing the results among Tables S3–S5 (Supporting Information). As shown in Table S3 (Supporting Information), the RMSD of HF/3-21+G* from its dual-level CCSD(T) counterpart is obviously the largest, at the huge value of 8 kcal/mol, and the same largest huge value of 8 kcal/mol is also found in Table S4 (Supporting Information) that lists RMSD of all six single levels of calculations with respect to CCSD(T)/6-311+G(d,p)//MP2/6-311+G(d,p) (which should be the most accurate level of theory considered in this article). However, the RMSD between the dual-level CCSD(T) of HF/3-21+G* and the dual-level CCSD(T) of MP2/6-311+G(d,p) is only 0.4 kcal/mol, which is (tied at) the smallest value comparing to all other four levels of theory listed in Table S5 (Supporting Information). All these striking results about dual-level calculations could serve as an important precursor towards some future work of high-level and affordable on-the-fly *ab initio* QM/MM free-energy simulations for actual RNA catalysis. This is because oftentimes even in molecular simulations, it could be possible to treat the entire active site on the fly at the HF/3-21+G* level for the purpose of sampling the phase space. Subsequently, we could systematically refine the *ab initio* QM/MM free-energy profile by means of a free-energy perturbation method with a small number of high-level calculations.

According to Tables S3–S5 (Supporting Information), the overall performances of two popular density functionals, B3LYP and M06-2X, are quite similar (and definitely better than single-level HF/3-21+G*), though B3LYP might have the edge, in particular M06-2X tends to overstabilize the transient

**Table 4.** Most relevant available experimental results of native reactions in solution to compare with the calculated barriers of our simplest models of RNA phosphate transesterification.[a]

| | Liu et al.[b] | | Harris et al.[c] | | Iyer et al.[d] | | Thomson et al.[e] | | Weinstein et al.[f] | | Dantzman et al.[g] | |
|---|---|---|---|---|---|---|---|---|---|---|---|---|
| Native pH value | $t_{1/2}$[h] (min) | Barrier[i] (kcal/mol) | $t_{1/2}$[h] (min) | Barrier[i] (kcal/mol) | $t_{1/2}$[h] (min) | Barrier[i] (kcal/mol) | $t_{1/2}$[h] (min) | Barrier[i] (kcal/mol) | $t_{1/2}$[h] (min) | Barrier[i] (kcal/mol) | $t_{1/2}$[h] (min) | Barrier[i] (kcal/mol) |
| 8 | – | – | 54266 | 27.6 | – | – | – | – | – | – | 12[j] | 21.5 |
| 9 | – | – | 5427 | 26.2 | – | – | – | – | – | – | – | – |
| 10 | – | – | 543 | 24.8 | – | – | – | – | 7289[k] | 24.1 | – | – |
| 10.06 | 4800[l] | 27.3[l] | 473 | 24.7 | – | – | – | – | – | – | – | – |
| 11 | – | – | 54 | 23.4 | – | – | – | – | 729[m] | 22.8 | – | – |
| 11.5 | – | – | 17 | 22.7 | – | – | 825 | 25.1 | – | – | – | – |
| 12 | – | – | 6 | 22.0 | – | – | – | – | – | – | – | – |
| 13 | – | – | 0.7 | 20.7 | – | – | – | – | 37[n] | 21.1 | – | – |
| Infinity | – | – | 0.2 | 19.9 | – | – | – | – | – | – | – | – |

[a] "–" denotes the experimental data could not be found by us. [b] 50°C, UpU, Ref. [90–92]. [c] 37°C, UpG, Eq. (1) in Ref. [14]. [d] 80 °C, mNB, Ref. [93]. [e] 37°C, UpU, Ref. [94]. [f] 10°C, IpU, Ref. [95]. [g] 25°C, UppNp, Ref. [96]. [h] If the time of half life ($t_{1/2}$) is not given in the reference papers, then $t_{1/2}$ is derived from the first-order rate constant $k$ as follows: $t_{1/2}=(\ln 2)/k$. [i] The energy barrier is converted from the rate constant by conventional transition-state theory. [j] The extracted value of $k$ is $\sim 10^{-3}$ $s^{-1}$, from the Figure 3 in Ref. [96]. [k] The extracted value of $k$ is $\sim 10^{-5.8}$ $s^{-1}$, from the Figure 4 in Ref. [95]. [l] From 4800 to 5400 min, 27.3 to 27.4 kcal/mol. [m] The extracted value of $k$ is $\sim 10^{-4.8}$ $s^{-1}$, from the Figure 4 in Ref. [95]. [n] The extracted value of $k$ is $\sim 10^{-3.5}$ $s^{-1}$, from the Figure 4 in Ref. [95].

intermediates for both native and S3′ reactions quite a bit (Table 2). Interestingly, increasing the size of basis set from 6-31+G(d) to 6-311+G(d,p) does not necessarily increase the accuracy for both B3LYP and M06-2X functionals at either single [Table S4 (Supporting Information)] or dual levels [Table S5 (Supporting Information)]; however, their respective dual-level counterparts with single-point energy of CCSD(T)/6-311+G(d,p) still oftentimes improve the accuracy of the single level [Table S3 (Supporting Information)]. Note that the M06-2X overstabilization of the transient intermediates in both gas and solution phases has been generally rescued by dual-level calculations, but the dual-level energy for the native intermediate minimized at the M06-2X/6-31+G(d) ($\Delta G_{\text{Int}}$ = 17.3 kcal/mol) somehow is higher than the corresponding dual-level energy for the ETS ($\Delta G^{\ddagger}_{\text{ETS}}$ = 17.1 kcal/mol) by about 0.2 kcal/mol (Table 3). In comparison, for the case of the dual-level CCSD(T) of MP2/6-311+G(d,p) (i.e., the most accurate level considered in this article), the energy of the metastable native intermediate ($\Delta G_{\text{Int}}$ = 17.5 kcal/mol) is actually about 0.1 kcal/mol lower than the ETS ($\Delta G^{\ddagger}_{\text{ETS}}$ = 17.6 kcal/mol) (Table 3).

CCSD(T) is generally considered as "gold standard".[45,50,51] By comparing Table 3 with Table S2 (Supporting Information), we can see that the performance of the single-point-energy calculations at the CCSD level [without (T)] is actually not that close to those at the CCSD(T) level. In Table S6 (Supporting Information), we lists the RMSD between single-level calculations, and their respective counterparts of dual-level calculations that have single-point energy of CCSD/6-311+G(d,p). In contrast to the case for CCSD(T) shown in Table S3 (Supporting Information), this time for CCSD, no level of theory can

**Table 5.** Most relevant available experimental results of S3′ reactions in solution to compare with the calculated barriers of our simplest models of RNA phosphate transesterification.[a]

| | Liu et al.[b] | | Harris et al.[c] | | Iyer et al.[d] | | Thomson et al.[e] | | Weinstein et al.[f] | | Dantzman et al.[g] | |
|---|---|---|---|---|---|---|---|---|---|---|---|---|
| S3′ pH value | $t_{1/2}$[h] (min) | Barrier[i] (kcal/mol) | $t_{1/2}$[h] (min) | Barrier[i] (kcal/mol) | $t_{1/2}$[h] (min) | Barrier[i] (kcal/mol) | $t_{1/2}$[h] (min) | Barrier[i] (kcal/mol) | $t_{1/2}$[h] (min) | Barrier[i] (kcal/mol) | $t_{1/2}$[h] (min) | Barrier[i] (kcal/mol) |
| 8 | – | – | – | – | – | – | – | – | – | – | – | – |
| 9 | – | – | – | – | 11552[j] | 30.5 | – | – | – | – | – | – |
| 10 | – | – | – | – | 5403[k] | 30.0 | – | – | 7[l] | 20.2 | – | – |
| 10.06 | 25 | 23.9 | – | – | – | – | – | – | – | – | – | – |
| 11 | – | – | – | – | 650[m] | 28.5 | – | – | 0.4[n] | 18.5 | – | – |
| 11.5 | – | – | – | – | 249[o] | 27.8 | – | – | – | – | – | – |
| 12 | – | – | – | – | 87[p] | 27.1 | – | – | – | – | – | – |
| 13 | – | – | – | – | 20.5[q] | 26.0 | – | – | 0.02[r] | 16.8 | – | – |
| Infinity | – | – | – | – | – | – | – | – | – | – | – | – |

[a] "–" denotes the experimental data could not be found by us. [b] 50°C, UspU, Ref. [90–92]. [c] 37°C, UspG, Eq. (1) in Ref. [14]. [d] 80°C, S3′mNB, Ref. [93]. [e] 37°C, UspU, Ref. [94]. [f] 10°C, IspU, Ref. [95]. [g] 25°C, UsppNp, Ref. [96]. [h] If the time of half life ($t_{1/2}$) is not given in the reference papers, then $t_{1/2}$ is derived from the first-order rate constant $k$ as follows: $t_{1/2}=(\ln 2)/k$. [i] The energy barrier is converted from the rate constant by conventional transition state theory. [j] The extracted value of $k$ is $\sim 10^{-6}$ $s^{-1}$, from Supporting Information, Figure S2 in Ref. [93]. [k] The extracted value of $k$ is $\sim 10^{-5.67}$ $s^{-1}$, from Supporting Information, Figure S2 in Ref. [93]. [l] The extracted value of $k$ is $\sim 10^{-2.8}$ $s^{-1}$, from Supporting Information, Figure 4 in Ref. [95]. [m] The extracted value of $k$ is $\sim 10^{-4.75}$ $s^{-1}$, from Supporting Information, Figure S2 in Ref. [93]. [n] The extracted value of $k$ is $\sim 10^{-1.5}$ $s^{-1}$, from Supporting Information, Figure 4 in Ref. [95]. [o] The extracted value of $k$ is $\sim 10^{-4.33}$ $s^{-1}$, from Supporting Information, Figure S2 in Ref. [93]. [p] The extracted value of $k$ is $\sim 10^{-3.875}$ $s^{-1}$, from Supporting Information, Figure S2 in Ref. [93]. [q] The extracted value of $k$ is $\sim 10^{-3.25}$ $s^{-1}$, from Supporting Information, Figure S2 in Ref. [93]. [r] The extracted value of $k$ is $\sim 10^{-0.2}$ $s^{-1}$, from Supporting Information, Figure 4 in Ref. [95].

**Table 6.** Most relevant available experimental results of S5′ reactions in solution to compare with the calculated barriers of our simplest models of RNA phosphate transesterification.[a]

| | Liu et al.[b] | | Harris et al.[c] | | Iyer et al.[d] | | Thomson et al.[e] | | Weinstein et al.[f] | | Dantzman et al.[g] | |
|---|---|---|---|---|---|---|---|---|---|---|---|---|
| S5′ pH value | $t_{1/2}$[h] (min) | Barrier[i] (kcal/mol) | $t_{1/2}$[h] (min) | Barrier[i] (kcal/mol) | $t_{1/2}$[h] (min) | Barrier[i] (kcal/mol) | $t_{1/2}$[h] (min) | Barrier[i] (kcal/mol) | $t_{1/2}$[h] (min) | Barrier[i] (kcal/mol) | $t_{1/2}$[h] (min) | Barrier[i] (kcal/mol) |
| 8 | 132 | 23.4 | – | – | 9176[j] | 30.3 | 46[p] | 23.3 | – | – | – | – |
| 9 | 29 | 22.5 | – | – | 6496[k] | 30.1 | 4 | 21.7 | – | – | – | – |
| 10 | – | – | – | – | 1155[l] | 28.9 | – | – | – | – | – | – |
| 10.06 | – | – | – | – | – | – | – | – | – | – | – | – |
| 11 | – | – | – | – | 116[m] | 27.3 | – | – | – | – | – | – |
| 11.5 | – | – | – | – | 32.6[n] | 26.4 | – | – | – | – | – | – |
| 12 | – | – | – | – | 15.4[o] | 25.8 | – | – | – | – | – | – |
| 13 | – | – | – | – | – | – | – | – | – | – | – | – |
| Infinity | – | – | – | – | – | – | – | – | – | – | – | – |

[a] "–" denotes the experimental data could not be found by us. [b] 30°C, UpsU, Ref. [90–92]. [c] 37°C, UpsG, Eq. (1) in Ref. [14]. [d] 80°C, S5′mNB, Ref. [93]. [e] 37°C, UpsU, Ref. [94]. [f] 10°C, IpsU, Ref. [95]. [g] 25°C, UpspNp, Ref. [96]. [h] If the time of half life ($t_{1/2}$) is not given in the reference papers, then $t_{1/2}$ is derived from the first order rate constant $k$ as follows: $t_{1/2}=(\ln 2)/k$. [i] The energy barrier is converted from the rate constant by conventional transition state theory. [j] The extracted value of $k$ is $\sim 10^{-5.9}$ $s^{-1}$, from Supporting Information, Figure S3 in Ref. [93]. [k] The extracted value of $k$ is $\sim 10^{-5.75}$ $s^{-1}$, from Supporting Information, Figure S3 in Ref. [93]. [l] The extracted value of $k$ is $\sim 10^{-5}$ $s^{-1}$, from Supporting Information, Figure S3 in Ref. [93]. [m] The extracted value of $k$ is $\sim 10^{-4}$ $s^{-1}$, from Supporting Information, Figure S3 in Ref. [93]. [n] The extracted value of $k$ is $\sim 10^{-3.45}$ $s^{-1}$, from Supporting Information, Figure S3 in Ref. [93]. [o] The extracted value of $k$ is $\sim 10^{-3.125}$ $s^{-1}$, from Supporting Information, Figure S3 in Ref. [93]. [p] The extracted value of $k$ is $\sim 10^{-3.6}$ $s^{-1}$, from Figure 2 in Ref. [94].

have RMSD smaller than 1 kcal/mol [Table S6 (Supporting Information)]. Moreover, from Table S7 (Supporting Information), all six dual-level calculations with single-point energy of CCSD/6-311+G(d,p) exhibit RMSD of ~1–2 kcal/mol from our most accurate level of theory: CCSD(T)/6-311+G(d,p)//MP2/6-311+G(d,p). Nonetheless, the computational cost of CCSD(T) is about two and a half times as much as the CCSD.

With regard to the agreement between the calculated barriers with experiment, in Tables 4–6, we present the most relevant available experimental results that we have found in the literature for the native, S3′, and S5′ reactions in solution. Note that none of experimental results shown in Tables 4–6 is the actual methanolysis of ethylene phosphate that we calculated in this article (Scheme 1). Most of the experiments are RNA transphosphorylation of dinucleotides with different combinations of the nucleobases, and often under different experimental conditions.

Nevertheless, by comparing the experimental results of the IpU and IspU reactions measured by Weinstein et al.,[95] we could conclude that in general S3′ reactions should be faster than the native ones. Similarly, by comparing the experimental results of the S3′mNB and S5′mNB reactions measured by Iyer and Hengge,[93] we could also conclude that in general S5′ reactions should be faster than S3′ reactions by just a little bit. These two conclusions are consistent with our calculated results (Tables 2 and 3).

### Breaking/forming bond orders and bond distances

As indirectly suggested by the minimal values of dual-level RMSD in Table S5 (Supporting Information), all values of breaking/forming bond orders and bond distances associated with the transition states shown in Table 7, Table S8 (Supporting Information), and Table 8 (which are all either calculated at

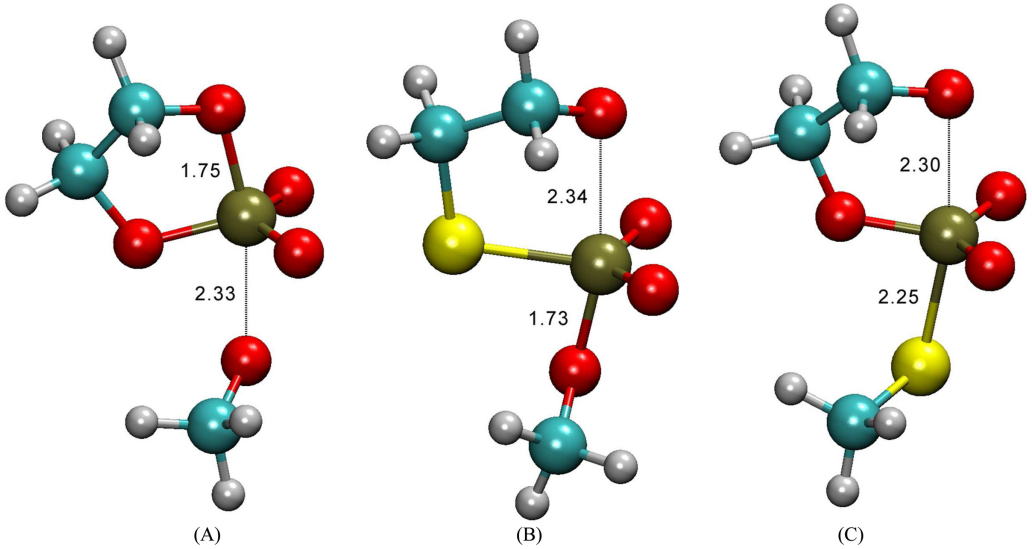


**Figure 2.** Rate-limiting transition-state structures that match with experimental KIE values for the (A) native, (B) S3′, (C) S5′ reactions, respectively. These structures were optimized at the MP2/6-311+G(d,p) level. The bond distances are given in Å.

**Table 7.** Single-level Wiberg bond order (bond index) for stationary points along the intrinsic reaction coordinate of the (A) native, (B) S3′, and (C) S5′ simplest models of RNA transphosphorylation in both gas and solution phases.[a]

| | Gas (Å) | | | | | | Solution (Å) | | | | | |
|---|---|---|---|---|---|---|---|---|---|---|---|---|
| | ETS | | Int | | LTS | | ETS | | Int | | LTS | |
| Electronic structure theory | $BO_{X5'}$[b] | $BO_{O2'}$ | $BO_{O5'}$ | $BO_{O2'}$ | $BO_{O5'}$ | $BO_{O2'}$ | $BO_{X5'}$[b] | $BO_{O2'}$ | $BO_{O5'}$ | $BO_{O2'}$ | $BO_{O5'}$ | $BO_{O2'}$ |
| (A) Native | | | | | | | | | | | | |
| HF/3-21+G* | – | – | – | – | 0.11 | 0.47 | 0.52 | 0.28 | 0.48 | 0.41 | 0.18 | 0.53 |
| B3LYP/6-31+G(d) | – | – | – | – | 0.15 | 0.44 | 0.50 | 0.29 | 0.47 | 0.40 | 0.21 | 0.52 |
| M06-2X/6-31+G(d) | – | – | – | – | 0.12 | 0.46 | 0.53 | 0.20 | 0.46 | 0.42 | 0.16 | 0.53 |
| B3LYP/6-311+G(d,p) | – | – | – | – | 0.14 | 0.45 | 0.51[c] | 0.33[c] | _[d] | _[d] | 0.20 | 0.54 |
| M06-2X/6-311+G(d,p) | – | – | – | – | 0.10 | 0.48 | 0.55 | 0.21 | 0.49 | 0.42 | 0.14 | 0.56 |
| MP2/6-311+G(d,p) | – | – | – | – | 0.09 | 0.46 | 0.52 | 0.24 | 0.47 | 0.39 | 0.14 | 0.53 |
| (B) S3′ | | | | | | | | | | | | |
| HF/3-21+G* | 0.49 | 0.15 | _[d] | _[d] | 0.14 | 0.49 | 0.54 | 0.19 | 0.45 | 0.45 | 0.18 | 0.54 |
| B3LYP/6-31+G(d) | 0.47 | 0.23 | 0.43 | 0.43 | 0.19 | 0.47 | 0.52 | 0.22 | 0.44 | 0.43 | 0.20 | 0.53 |
| M06-2X/6-31+G(d) | 0.49 | 0.15 | 0.44 | 0.44 | 0.11 | 0.49 | 0.53 | 0.16 | 0.44 | 0.44 | 0.14 | 0.54 |
| B3LYP/6-311+G(d,p) | 0.47 | 0.23 | 0.43 | 0.42 | 0.19 | 0.48 | 0.53 | 0.22 | 0.45 | 0.43 | 0.20 | 0.54 |
| M06-2X/6-311+G(d,p) | 0.51 | 0.13 | 0.44 | 0.45 | 0.10 | 0.51 | 0.56 | 0.15 | 0.46 | 0.45 | 0.13 | 0.57 |
| MP2/6-311+G(d,p) | 0.48 | 0.14 | 0.42 | 0.42 | 0.12 | 0.47 | 0.53 | 0.14 | 0.44 | 0.43 | 0.14 | 0.53 |
| (C) S5′ | | | | | | | | | | | | |
| HF/3-21+G* | 0.48 | 0.16 | – | – | – | – | 0.72 | 0.20 | – | – | – | – |
| B3LYP/6-31+G(d) | 0.41 | 0.18 | – | – | – | – | 0.66 | 0.22 | – | – | – | – |
| M06-2X/6-31+G(d) | 0.50 | 0.16 | – | – | – | – | 0.68 | 0.18 | – | – | – | – |
| B3LYP/6-311+G(d,p) | 0.39 | 0.17 | – | – | – | – | 0.65 | 0.22 | – | – | – | – |
| M06-2X/6-311+G(d,p) | 0.49 | 0.15 | – | – | – | – | 0.67 | 0.18 | – | – | – | – |
| MP2/6-311+G(d,p) | 0.45 | 0.16 | – | – | – | – | 0.71 | 0.16 | – | – | – | – |

[a] $BO_{O5'}$ is the bond order between O5′ and P, $BO_{O2'}$ is the bond order between O2′ and P, $BO_{S5'}$ is the bond order between S5′ and P. "–" denotes the molecular structure of that particular state could not be determined by us. [b] X = O for native and S3′; X = S for S5′. [c] As in Table 2, the ETS is determined but along with very small value of nonreactive imaginary frequency. [d] As in Table 2, no minimum point could be determined by us that satisfies all default criteria in GAUSSIAN 09.[41]

**Table 8.** Breaking and forming bond distances for stationary points along the intrinsic reaction coordinate of the (A) native, (B) S3′, and (C) S5′ simplest models of RNA transphosphorylation in both gas and solution phases.[a]

| | Gas (Å) | | | | | | Solution (Å) | | | | | |
|---|---|---|---|---|---|---|---|---|---|---|---|---|
| | ETS | | Int | | LTS | | ETS | | Int | | LTS | |
| Electronic structure theory | $r_{X5'}$[b] | $r_{O2'}$ | $r_{O5'}$ | $r_{O2'}$ | $r_{O5'}$ | $r_{O2'}$ | $r_{X5'}$[b] | $r_{O2'}$ | $r_{O5'}$ | $r_{O2'}$ | $r_{O5'}$ | $r_{O2'}$ |
| (A) Native | | | | | | | | | | | | |
| HF/3-21+G* | – | – | – | – | 2.55 | 1.75 | 1.70 | 2.09 | 1.75 | 1.86 | 2.29 | 1.71 |
| B3LYP/6-31+G(d) | – | – | – | – | 2.49 | 1.84 | 1.77 | 2.13 | 1.82 | 1.93 | 2.31 | 1.77 |
| M06-2X/6-31+G(d) | – | – | – | – | 2.52 | 1.79 | 1.72 | 2.28 | 1.80 | 1.87 | 2.38 | 1.72 |
| B3LYP/6-311+G(d,p) | – | – | – | – | 2.49 | 1.85 | 1.78[c] | 2.05[c] | _[d] | _[d] | 2.30 | 1.77 |
| M06-2X/6-311+G(d,p) | – | – | – | – | 2.53 | 1.79 | 1.72 | 2.25 | 1.79 | 1.89 | 2.38 | 1.72 |
| MP2/6-311+G(d,p) | – | – | – | – | 2.52 | 1.82 | 1.75 | 2.15 | 1.80 | 1.92 | 2.33 | 1.75 |
| (B) S3′ | | | | | | | | | | | | |
| HF/3-21+G* | 1.72 | 2.41 | _[d] | _[d] | 2.38 | 1.72 | 1.68 | 2.30 | 1.78 | 1.80 | 2.28 | 1.69 |
| B3LYP/6-31+G(d) | 1.80 | 2.29 | 1.88 | 1.89 | 2.35 | 1.81 | 1.75 | 2.30 | 1.85 | 1.89 | 2.30 | 1.76 |
| M06-2X/6-31+G(d) | 1.75 | 2.46 | 1.83 | 1.83 | 2.51 | 1.75 | 1.70 | 2.40 | 1.81 | 1.83 | 2.41 | 1.71 |
| B3LYP/6-311+G(d,p) | 1.81 | 2.27 | 1.89 | 1.91 | 2.34 | 1.82 | 1.75 | 2.29 | 1.85 | 1.90 | 2.28 | 1.76 |
| M06-2X/6-311+G(d,p) | 1.75 | 2.47 | 1.84 | 1.84 | 2.52 | 1.75 | 1.70 | 2.40 | 1.81 | 1.84 | 2.42 | 1.71 |
| MP2/6-311+G(d,p) | 1.78 | 2.38 | 1.87 | 1.88 | 2.40 | 1.79 | 1.73 | 2.34 | 1.83 | 1.86 | 2.32 | 1.74 |
| (C) S5′ | | | | | | | | | | | | |
| HF/3-21+G* | 2.42 | 2.38 | – | – | – | – | 2.21 | 2.24 | – | – | – | – |
| B3LYP/6-31+G(d) | 2.57 | 2.41 | – | – | – | – | 2.29 | 2.31 | – | – | – | – |
| M06-2X/6-31+G(d) | 2.41 | 2.42 | – | – | – | – | 2.25 | 2.34 | – | – | – | – |
| B3LYP/6-311+G(d,p) | 2.60 | 2.41 | – | – | – | – | 2.31 | 2.29 | – | – | – | – |
| M06-2X/6-311+G(d,p) | 2.42 | 2.41 | – | – | – | – | 2.26 | 2.33 | – | – | – | – |
| MP2/6-311+G(d,p) | 2.49 | 2.35 | – | – | – | – | 2.25 | 2.30 | – | – | – | – |

[a] $r_{O5'}$ is the distance between O5′ and P, $r_{O2'}$ is the distance between O2′ and P, $r_{S5'}$ is the distance between S5′ and P. "–" denotes the molecular structure of that particular state could not be determined by us. [b] X = O for native and S3′; X = S for S5′. [c] As in Table 2, the ETS is determined but along with very small value of nonreactive imaginary frequency. [d] As in Table 2, no minimum point could be determined by us that satisfies all default criteria in GAUSSIAN 09.[41]

**Table 9.** Equilibrium isotope effects on nucleophile (2′-OH) deprotonation of the (A) native, (B) S3′, and (C) S5′ simplest models of RNA transphosphorylation in solution.[a]

| | Equilibrium isotope effects in solution (ratio of isotopic equilibrium constants) | | | | |
|---|---|---|---|---|---|
| | Nucleophile (2′-OH) deprotonation | | | | |
| Electronic structure theory | $^{18}E_{Nuc}$ | $^{18,34}E_{Lea}$ | $^{18,34}E_{X3'}$[b] | $^{18}E_{O1P}$ | $^{18}E_{O2P}$ |
| (A) Native (37°C) | | | | | |
| HF/3-21+G* | 1.0245 | 1.0020 | 0.9985 | 0.9991 | 0.9999 |
| B3LYP/6-31+G(d) | 1.0210 | 1.0007 | 1.0012 | 0.9999 | 1.0008 |
| M06-2X/6-31+G(d) | 1.0214 | 1.0015 | 0.9975 | 1.0000 | 0.9998 |
| B3LYP/6-311+G(d,p) | 1.0220 | 1.0007 | 1.0013 | 0.9997 | 1.0011 |
| M06-2X/6-311+G(d,p) | 1.0222 | 1.0016 | 0.9977 | 0.9999 | 1.0001 |
| MP2/6-311+G(d,p) | 1.0218 | 1.0020 | 0.9984 | 1.0004 | 1.0003 |
| (B) S3′ (37°C) | | | | | |
| HF/3-21+G* | 1.0266 | 1.0002 | 1.0000 | 1.0003 | 0.9995 |
| B3LYP/6-31+G(d) | 1.0196 | 1.0005 | 1.0003 | 1.0007 | 1.0006 |
| M06-2X/6-31+G(d) | 1.0244 | 1.0002 | 1.0009 | 1.0005 | 0.9998 |
| B3LYP/6-311+G(d,p) | 1.0208 | 1.0005 | 1.0003 | 1.0008 | 1.0006 |
| M06-2X/6-311+G(d,p) | 1.0255[c] | 1.0003[c] | 1.0009[c] | 1.0005[c] | 1.0000[c] |
| MP2/6-311+G(d,p) | 1.0271 | 1.0001 | 1.0007 | 1.0004 | 1.0004 |
| (C) S5′ (37°C) | | | | | |
| HF/3-21+G* | 1.0259 | 0.9997 | 1.0001 | 1.0002 | 1.0014 |
| B3LYP/6-31+G(d) | 1.0204 | 1.0002 | 1.0026 | 1.0011 | 1.0004 |
| M06-2X/6-31+G(d) | 1.0215 | 0.9994 | 1.0024 | 1.0005 | 1.0011 |
| B3LYP/6-311+G(d,p) | 1.0215 | 1.0002 | 1.0027 | 1.0012 | 1.0004 |
| M06-2X/6-311+G(d,p) | 1.0222 | 0.9993 | 1.0022 | 1.0004 | 1.0012 |
| MP2/6-311+G(d,p) | 1.0225 | 0.9999 | 1.0002 | 1.0004 | 1.0001 |

[a] All values are computed from the Bigeleisen equation. [b] X = O for native and S5′; X = S for S3′. [c] As in Table 2, the ground state after deprotonation (i.e., the dianionic reactant) is determined but along with very small value of non-reactive imaginary frequency.

single or dual levels) are in fact quite close to one another. They are all virtually within only 0.1 or 0.1 Å from one another for bond orders and distances, respectively. This finding further supports the aforementioned idea that it could be quite possible and accurate to have dual-level and systematic types of on-the-fly *ab initio* QM/MM free-energy simulations for actual RNA catalysis. Furthermore, according to the data shown in these three tables [Tables 7, S8 (Supporting Information), and 8], we have the same conclusions as in our previous study that the rate-limiting transition states for the native reactions in both gas and solution phases (which are LTS) exhibit cleavage of the exocyclic P—O5′ is advanced.[8,9] Take the MP2 structure of LTS in solution as an example, P—O5′ distance is 2.33 Å and its bond order is 0.14, whereas P—O2′ bond is at 1.75 Å and its bond order is 0.53 (Fig. 2).

On the other hand, the ETS for both S3′ and S5′ reactions in solution, which are the rate-limiting transition states in accordance with the experimental and calculated KIE data,[9] show the covalent bond between P—O2′ (the nucleophilic bond) is far from being formed (Fig. 2), in particular the fast leaving group of S5′ makes the LTS in the S5′ reaction extinct. For example, the MP2 structure of S3′-ETS in solution has the bond distance of P—O5′ at 1.73 Å and its bond order is 0.53, whereas the P—O2′ distance is 2.34 Å and its bond order is 0.14 (Fig. 2).

### EIE on 2′-OH deprotonation

In the base-catalyzed reaction mechanism, previously we showed that the O2′ has already been deprotonated in the reactant state.[9] However, during the actual RNA catalysis, we should have the 2′-OH for the ground state instead.[8] Therefore, it is of particular interest in determining the EIE on the 2′-OH deprotonation.[8,9,14,30]

Single levels and dual levels of EIE for our simplest native and thio-substituted models in the gas phase are listed in Tables S9 and S10 (Supporting Information), respectively. All these EIE values were computed from the Bigeleisen equation [Eq. (3)]. Because frequency analyses at coupled-cluster level are extremely expensive, and as what we have discussed above, CCSD(T)/6-311+G(d,p)//MP2/6-311+G(d,p) are the most accurate level of theory in this work, all the dual-level calculations of EIE and KIE in this work were performed with frequency analyses at the MP2/6-311+G(d,p) level.

Similar to the cases in breaking/forming bond orders and bond distances, the differences in EIE between the single-level values and their dual-level counterparts in the gas phase are basically insignificant [Table S9 vs. Table S10 (Supporting Information)]. For the gas-phase native reaction, the largest EIE is on the O2′ among all 12 single and dual levels of theory, ranging from 1.029 to 1.039, in which the MP2 EIE value is 1.031. The second largest EIE is on the O5′ ranging from 1.005 to 1.006 among all 12 single and dual levels of theory, in which the MP2 EIE value is 1.0059. The EIE values on the remaining phosphoryl oxygen are close to unity, ranging from 1.000 to 1.003, at all 12 single and dual levels of theory. Similar values of EIE can also be found for both S3′ and S5′ reactions in the gas phase, with a note that $^{18,34}E_{Lea}$ values are reduced to be in the range of 1.002.

For all the reactions in solution, as shown in Tables 9 and S11 (Supporting Information), the differences in EIE between the single-level values and their dual-level counterparts are

**Table 10.** Kinetic isotope effects on the (A) native, (B) S3′, and (C) S5′ simplest models of RNA transphosphorylation in solution.[a]

| | Kinetic isotope effects in solution (ratio of isotopic reaction rates) | | | | | | | | | |
|---|---|---|---|---|---|---|---|---|---|---|
| | ETS | | | | | LTS | | | | |
| Electronic structure theory | $^{18}k_{Nuc}$ | $^{18,34}k_{Lea}$ | $^{18,34}k_{X3'}$[b] | $^{18}k_{O1P}$ | $^{18}k_{O2P}$ | $^{18}k_{Nuc}$ | $^{18,34}k_{Lea}$ | $^{18,34}k_{X3'}$[b] | $^{18}k_{O1P}$ | $^{18}k_{O2P}$ |
| (A) Native (37°C) | | | | | | | | | | |
| HF/3-21+G* | 1.0105 | 1.0063 | 1.0022 | 1.0037 | 1.0046 | 0.9515 | 1.0805 | 1.0022 | 1.0038 | 1.0035 |
| B3LYP/6-31+G(d) | 1.0169 | 1.0064 | 1.0051 | 1.0041 | 1.0039 | 0.9673 | 1.0607 | 1.0051 | 1.0049 | 1.0026 |
| M06-2X/6-31+G(d) | 1.0239 | 1.0060 | 1.0040 | 1.0031 | 1.0023 | 0.9630 | 1.0716 | 1.0050 | 1.0039 | 1.0027 |
| B3LYP/6-311+G(d,p) | 1.0117[c] | 1.0078[c] | 1.0064[c] | 1.0049[c] | 1.0046[c] | 0.9677 | 1.0602 | 1.0057 | 1.0050 | 1.0024 |
| M06-2X/6-311+G(d,p) | 1.0229 | 1.0064 | 1.0043 | 1.0035 | 1.0026 | 0.9635 | 1.0719 | 1.0054 | 1.0042 | 1.0024 |
| MP2/6-311+G(d,p) | 1.0190 | 1.0075 | 1.0046 | 1.0047 | 1.0045 | 0.9665 | 1.0683 | 1.0043 | 1.0039 | 1.0029 |
| (B) S3′ (37°C) | | | | | | | | | | |
| HF/3-21+G* | 1.0209 | 1.0076 | 1.0007 | 1.0024 | 1.0023 | 0.9510 | 1.0697 | 1.0008 | 1.0019 | 1.0013 |
| B3LYP/6-31+G(d) | 1.0250 | 1.0086 | 1.0010 | 1.0033 | 1.0038 | 0.9709 | 1.0575 | 1.0014 | 1.0017 | 1.0026 |
| M06-2X/6-31+G(d) | 1.0276 | 1.0075 | 1.0010 | 1.0016 | 1.0024 | 0.9646 | 1.0714 | 1.0009 | 1.0007 | 1.0013 |
| B3LYP/6-311+G(d,p) | 1.0242 | 1.0092 | 1.0010 | 1.0034 | 1.0038 | 0.9713 | 1.0557 | 1.0015 | 1.0014 | 1.0021 |
| M06-2X/6-311+G(d,p) | 1.0277[d] | 1.0076[d] | 1.0011[d] | 1.0021[d] | 1.0021[d] | 0.9641[d] | 1.0723[d] | 1.0010[d] | 1.0007[d] | 1.0011[d] |
| MP2/6-311+G(d,p) | 1.0264 | 1.0088 | 1.0011 | 1.0035 | 1.0030 | 0.9659 | 1.0666 | 1.0013 | 1.0020 | 1.0024 |
| (C) S5′ (37°C) | | | | | | | | | | |
| HF/3-21+G* | 1.0150 | 1.0022 | 1.0036 | 1.0025 | 1.0033 | – | – | – | – | – |
| B3LYP/6-31+G(d) | 1.0198 | 1.0021 | 1.0051 | 1.0037 | 1.0037 | – | – | – | – | – |
| M06-2X/6-31+G(d) | 1.0203 | 1.0022 | 1.0027 | 1.0030 | 1.0016 | – | – | – | – | – |
| B3LYP/6-311+G(d,p) | 1.0187 | 1.0020 | 1.0056 | 1.0039 | 1.0039 | – | – | – | – | – |
| M06-2X/6-311+G(d,p) | 1.0196 | 1.0019 | 1.0035 | 1.0027 | 1.0018 | – | – | – | – | – |
| MP2/6-311+G(d,p) | 1.0211 | 1.0019 | 1.0064 | 1.0037 | 1.0040 | – | – | – | – | – |

[a] All values are computed from the Bigeleisen equation. "–" denotes the molecular structure of that particular state could not be determined by us. [b] X = O for native and S5′; X = S for S3′. [c] As in Table 2, the ETS is determined but along with very small value of non-reactive imaginary frequency. [d] As in Table 2, the reactant is determined but along with very small value of non-reactive imaginary frequency.

even more minimal. For the solution-phase native reaction, the largest EIE is still on the O2′ among all 12 single and dual levels of theory. But, comparing to their gas-phase counterparts, their EIE values on the O2′ in solution have been slightly reduced to be around 1.025, in which the MP2 value is 1.0218. These EIE values are similar to the EIE value, 1.0245, reported by Humphry et al. for deprotonation of the hydroxyl of 2-hydroxypropyl-*p*-nitrophenyl phosphate (HpPNP).[9,30]

Similar to the gas-phase results, the second largest EIE for the native reaction in solution is on the O5′, at the values of ~1.002, except the ones using B3LYP functional at the values of ~1.0007 [Tables 9 and S11 (Supporting Information)]. The EIE values on the remaining phosphoryl oxygen are also close to unity, ranging from 0.998 to 1.000, at all 12 single and dual levels of theory. Similar values of EIE can also be found for both S3′ and S5′ reactions in the solution phase, with a note that $^{18,34}E_{Lea}$ values are reduced to be ~1.000.

Remarkably, for the S5′ reaction in solution [Tables 9 and S11 (Supporting Information)], both single-level and dual-level calculations of EIE on the O3′ at the HF/3-21+G* level outperform the B3LYP and M06-2X functionals, in which the latter even have larger basis sets. The accurate MP2 value of EIE is 1.0002, whereas the HF values are ~1.0004. And the two functional values are not accurate, which are at the values of ~1.0020, off by one order of magnitude in terms of error percentage.

### KIE on RNA transphosphorylation

Similar to what we have discussed in the previous section for EIE, as frequency analyses at coupled-cluster level are prohibitively expensive and CCSD(T)/6-311+G(d,p)//MP2/6-311+G(d,p) are the most accurate level of theory in this study, all the dual-level calculations of EIE and KIE in this work were carried out with frequency analyses at the MP2/6-311+G(d,p) level.

Tables S12 and S13 (Supporting Information) list single and dual levels of KIE in the gas phase. All these KIE values were calculated from the Bigeleisen equation [Eq. (4)]. Similar to the calculations for EIE, for all reactions in the gas phase, we cannot find significant difference in the KIE values computed at the single levels from their dual-level counterparts. Moreover, all the KIE values computed at all 12 single and dual levels are actually quite close to one another. For the gas-phase native reaction, all the 12 KIE values of LTS on the O2′, O5′, O3′, O1P, and O2P are in the vicinities of 0.960, 1.070, 1.005, 1.001, and 1.001, respectively, in which the MP2 KIE values are 0.9727, 1.0669, 1.0084, 1.0011, and 0.9999, respectively. For the gas-phase S3′ reaction, all the KIE values of ETS on the O2′, O5′, S3′, O1P, and O2P are in the vicinities of 1.025, 1.010, 1.002, 1.001, and 1.001, respectively, in which the MP2 KIE values are 1.0250, 1.0115, 1.0024, 1.0009, and 1.0008, respectively. In addition, the KIE of LTS on the O2′, O5′, S3′, O1P, and O2P are in the ranges of 0.960, 1.060, 1.003, 1.001, and 1.001, respectively, in which the MP2 KIE values are 0.9738, 1.0591, 1.0041, 1.0013, and 1.0009, respectively. For the gas-phase S5′ reaction, all the KIE values of ETS on the O2′, S5′, O3′, O1P, and O2P are in the ranges of 1.015, 1.005, 1.002, 1.000, and 1.000, respectively, in which the MP2 KIE values are 1.0117, 1.0051, 1.0030, 1.0002, and 1.0010, respectively.

On the other hand, Tables 10 and S14 (Supporting Information) show single and dual levels of KIE in solution. Once again,

**Table 11.** *Ab initio* path-integral calculations of equilibrium isotope effects on nucleophile (2′-OH) deprotonation of the (A) native, (B) S3′, and (C) S5′ simplest models of RNA transphosphorylation in solution.[a]

| | *Ab initio* path-integral calculations | |
|---|---|---|
| Electronic structure theory MP2/6-311+G(d,p) | $^{18}E_{Nuc}$ | $^{18,34}E_{Lea}$ |
| (A) Native (37°C) | | |
| Full harmonic | 1.0218 | 1.0020 |
| Partial harmonic | 1.0212 | 1.0020 |
| Partial KP1/P20 | 1.0273 | 1.0044 |
| Partial KP2/P20 | 1.0261 | 1.0044 |
| Full harmonic × partial(KP1/harmonic) | 1.0279 | 1.0045 |
| Full harmonic × partial(KP2/harmonic) | 1.0268 | 1.0044 |
| (B) S3′ (37°C) | | |
| Full harmonic | 1.0271 | 1.0001 |
| Partial harmonic | 1.0266 | 1.0001 |
| Partial KP1/P20 | 1.0230 | 1.0005 |
| Partial KP2/P20 | 1.0224 | 1.0005 |
| Full harmonic × partial(KP1/harmonic) | 1.0235 | 1.0005 |
| Full harmonic × partial(KP2/harmonic) | 1.0228 | 1.0005 |
| (C) (S5′ (37°C) | | |
| Full harmonic | 1.0225 | 0.9999 |
| Partial harmonic | 1.0220 | 0.9999 |
| Partial KP1/P20 | 1.0194 | 0.9997 |
| Partial KP2/P20 | 1.0186 | 0.9997 |
| Full harmonic × partial(KP1/harmonic) | 1.0199 | 0.9997 |
| Full harmonic × partial(KP2/harmonic) | 1.0191 | 0.9997 |

[a] "Full harmonic" is the value computed from the Bigeleisen equation, in which the entire system is quantized. "Partial" means only six or seven nuclei are further quantized to compute the anharmonicity, which is excluded in the Bigeleisen equation. See Computational Details for the meanings of the notations of KP1/KP2 and P20.

we cannot find significant difference in the KIE values computed at the single levels from their dual-level counterparts. Further, again, all the KIE values computed at all 12 single and dual levels are in excellent agreement with one another. As what we conclude in the previous study,[9] by comparing our KIE values to the most relevant experimental KIE data, we have determined that the rate-limiting transition state for the native reaction is LTS, whereas for the S3′, and S5′ reactions are ETS.

For the solution-phase native reaction, the 12 KIE values of LTS on the O2′, O5′, O3′, O1P, and O2P are in the ranges of 0.960, 1.070, 1.004, 1.004, and 1.003, respectively, in which the MP2 KIE values are 0.9665, 1.0683, 1.0043, 1.0039, and 1.0029, respectively [Tables 10 and S14 (Supporting Information)]. For the solution-phase S3′ reaction, the 12 KIE values of ETS on the O2′, O5′, S3′, O1P, and O2P are in the vicinities of 1.025, 1.008, 1.001, 1.002, and 1.002, respectively, in which the MP2 KIE values are 1.0264, 1.0088, 1.0011, 1.0035, and 1.0030, respectively [Tables 10 and S14 (Supporting Information)]. For the solution-phase S5′ reaction, the 12 KIE values of ETS on the O2′, S5′, O3′, O1P, and O2P are in the vicinities of 1.020, 1.002, 1.004, 1.003, and 1.003, respectively, in which the MP2 KIE values are 1.0211, 1.0019, 1.0064, 1.0037, and 1.0040, respectively [Tables 10 and S14 (Supporting Information)].

Overall, impressively, EIE and KIE calculations at the HF/3-21+G* level are at least semiquantitatively accurate, even with no need to perform extra MP2 frequency analysis. Once again, this finding strongly indicates that systematic and dual-level on-the-fly *ab initio* QM/MM free-energy simulations for actual RNA catalysis could be very promising, even for EIE and KIE calculations.

Another fascinating finding for our EIE and KIE calculations can be located by comparing the values in the gas phase with those in solution [Table 10 vs. Table S12 (Supporting Information)]. Even though the solvent effects considerably reduce the energy barriers by at least ~10 kcal/mol to at most ~29 kcal/mol (Table 2), the intrinsic or the gas-phase EIE and KIE values are only marginally affected by the aqueous environment.

### Beyond the Bigeleisen equations: *Ab initio* path-integral calculations of EIE and KIE

Tables 11 and 12, S15, and S16 (Supporting Information) show primary EIE and KIE values computed with our path integral (PI) method, AIF-PI, for going beyond the Bigeleisen equations. The potential energy surface is constructed at the *ab initio* electronic-structure level of MP2/6-311+G(d,p) theory, which is the most accurate single level of theory we considered in this work. Our AIF-PI method, which is based on the impressively powerful and accurate Kleinert's variational perturbation (KP) theory, can systematically include the anharmonicity and tunneling effects in EIE and KIE calculations [i.e., Eqs. (5) and (6)]. Otherwise, the anharmonicity and tunneling effects are ignored in the widely used Bigeleisen equations [i.e., Eqs. (3) and (4)]. Our previous studies on a series of proton-transfer reactions demonstrate that performing *ab initio* PI calculations with our AIF-PI method can accurately and economically include anharmonicity and tunneling contributions to the KIE values calculated from Eq. (6). These two contributions are important to have quantitative agreement with experiment.[18,19,22] In this work, although the entire system is quantized for computing the harmonic EIE and KIE values, we only further quantize six or seven nuclei to estimate the anharmonic and tunneling effects. More information on our AIF-PI method is available in the section of Computational Details.

Based on the EIE and KIE values presented in Tables 11 and 12, S15, and S16 (Supporting Information), we conclude that further quantizing only six or seven nuclei should be enough for estimating the anharmonicity and tunneling effects. This is because the largest difference between the full harmonic (entire system is quantized) and partial harmonic (only six or seven nuclei are quantized) values is about 0.3% (in computing $^{18}k_{Nuc}$ value for the S5′ reaction in solution; Table 12). Moreover, even the largest tunneling contribution to the KIE values is only about 0.04% (in computing $^{18}k_{Nuc}$ value for the S5′ reaction in solution; Table 12). And most of our other calculated values of tunneling contributions are actually smaller than the largest 0.04% by at least one order of magnitude. In some cases, the imaginary frequency (for tunneling) is so small that once we quantize only six nuclei, no imaginary frequency can be found. Therefore, for simplicity, we do not explicitly list the KIE tunneling contributions in the tables (i.e., tunneling contributions are all implicitly included in the anharmonicity calculations).

Regarding the contributions from anharmonicity, we conclude that it is more quantitatively significant to EIE than KIE calculations. This finding is consistent with the fact that there is a

**Table 12.** *Ab initio* path-integral calculations of kinetic isotope effects on the (A) native, (B) S3′, and (C) S5′ simplest models of RNA transphosphorylation in solution.[a]

| | *Ab initio* path-integral calculations | | | |
|---|---|---|---|---|
| | ETS | | LTS | |
| Electronic structure theory: MP2/6-311+G(d,p) | $^{18}k_{Nuc}$ | $^{18,34}k_{Lea}$ | $^{18}k_{Nuc}$ | $^{18}k_{Lea}$ |
| (A) Native (37°C) | | | | |
| Full harmonic | 1.0190 | 1.0075 | 0.9665 | 1.0683 |
| Partial harmonic | 1.0207 | 1.0067 | 0.9680 | 1.0685 |
| Partial KP1/P20 | 1.0205 | 1.0048 | 0.9682 | 1.0659 |
| Partial KP2/P20 | 1.0205 | 1.0048 | 0.9681 | 1.0660 |
| Full harmonic × partial(KP1/harmonic) | 1.0189 | 1.0056 | 0.9667 | 1.0657 |
| Full harmonic × partial(KP2/harmonic) | 1.0188 | 1.0056 | 0.9666 | 1.0658 |
| (B) S3′ (37°C) | | | | |
| Full harmonic | 1.0264 | 1.0088 | 0.9659 | 1.0666 |
| Partial harmonic | 1.0287 | 1.0085 | 0.9673 | 1.0659 |
| Partial KP1/P20 | 1.0285 | 1.0072 | 0.9667 | 1.0658 |
| Partial KP2/P20 | 1.0285 | 1.0073 | 0.9667 | 1.0658 |
| Full harmonic × partial(KP1/harmonic) | 1.0262 | 1.0076 | 0.9653 | 1.0665 |
| Full harmonic × partial(KP2/harmonic) | 1.0262 | 1.0077 | 0.9653 | 1.0666 |
| (C) S5′ (37°C) | | | | |
| Full harmonic | 1.0211 | 1.0019 | – | – |
| Partial harmonic | 1.0243 | 1.0018 | – | – |
| Partial KP1/P20 | 1.0245 | 1.0019 | – | – |
| Partial KP2/P20 | 1.0245 | 1.0019 | – | – |
| Full harmonic × partial(KP1/harmonic) | 1.0213 | 1.0019 | – | – |
| Full harmonic × partial(KP2/harmonic) | 1.0213 | 1.0019 | – | – |

[a] "Full harmonic" is the value computed from the Bigeleisen equation, in which the entire system is quantized. "Partial" means only six nuclei are further quantized to compute the anharmonicity and tunneling effects, which are excluded in the Bigeleisen equation. See Computational Details for the meanings of the notations of KP1/KP2 and P20. "–" denotes the molecular structure of that particular state could not be determined by us.

hydrogen nucleus further quantized in the anharmonic EIE calculation. But for the KIE calculations, all six nuclei that are further quantized are heavy. We found that the largest anharmonic contribution is about 1% in computing $^{18}E_{Nuc}$ for both S3′ and S5′ reactions in the gas phase [Table S15 (Supporting Information)]. For all the reactions in the solution phase, the largest anharmonic contribution is about 0.5% in computing $^{18}E_{Nuc}$ for the native reaction in solution (Table 11). In contrast, the anharmonicity contributions to the KIE values are smaller. For all the reactions in both gas and solution phases, the largest anharmonic contribution is about 0.25% in computing $^{18}k_{Lea}$ value for the LTS of the native reaction in solution (Table 12).

The convergence of the KP1 and KP2 calculations are phenomenal. The largest difference between KP1 and KP2 values are in $^{18}E_{Nuc}$ calculations, for the reactions in solution, which is only about 0.1% (Table 11). For all other EIE and KIE calculations, their difference is smaller than or in the order of magnitude of 0.01% (Tables 11 and 12). Since KP theory has been well-known for its exponentially and uniformly convergent property (which is even true at the limit of absolute zero temperature and at the electronic scale), we believe that our PI calculations up to KP2 should be quite accurate.

Overall, in contrast to our previous studies on a series of proton-transfer reactions,[22] we found that as all our isotope effects are on heavy nuclei, in general anharmonicity and tunneling contributions are not significant to both EIE and KIE on our simplest models of RNA transphosphorylation. However, to have better quantitative agreement with experiment, we might need to include anharmonic contribution to the EIE calculations for the nucleophile (2′-OH) deprotonation, as there is a hydrogen nucleus directly bonded with the nucleophile O2′. For example, after adding the anharmonic contribution, now the $^{18}E_{Nuc}$ for the native reaction in solution is increased from 1.0218 to 1.0268 (Table 11).

## Conclusions

In this comprehensive article, we thoroughly compare various levels of electronic-structure and internuclear quantum-statistical theories for KIE and EIE computations on a simplest model for the base-catalyzed 2′-*O*-transphosphorylation. We find that in terms of energetics, MP2/6-311+G(d,p) is the most accurate single-level theory that we considered in this work [Table S3 (Supporting Information)]. Its RMSD from its dual-level counterpart that has single-point energy of CCSD(T)/6-311+G(d,p) is only 0.2 kcal/mol (0.3 kcal/mol is the largest deviation). Although the accuracy of the computationally least expensive HF/3-21+G* is generally not good enough [Table S4 (Supporting Information)], its dual-level CCSD(T) counterpart provides us with one of the most accurate results [Table S5 (Supporting Information)]. For density functional theory (DFT), in general, the performances of two popular functionals B3LYP and M06-2X are similar, but B3LYP might be a bit more accurate and M06-2X tends to overstabilize the transient intermediate for both native and S3′ reactions (in the gas and solution phases). Notably, CCSD and CCSD(T) results differ nontrivially, emphasizing the importance of the perturbative triple correction [Table S7 (Supporting Information)], while the computing time of CCSD(T) is longer than that of CCSD by a

factor of ~2.5 (Table 1). All the computed energy barriers for the native, S3′, and S5′ reactions are consistent with the most relevant experimental results that we have found in the literature, that is, S3′ reactions are faster than the natives ones, whereas the fastest reactions belong to the S5′ (Tables 2–6). Regarding the breaking/forming bond orders and bond distances associated with the transition states, all the values calculated at the single or dual levels are more or less the same as one another [Tables 7, S8 (Supporting Information), and 8].

For the calculations of the EIE on the 2′-OH deprotonation, we could not find important differences between the single-level and dual-level values in the gas phase, as well as in the solution phase [Table S9, S10 (Supporting Information), 9, and S11 (Supporting Information)]. Terrifically, for the S5′ reaction in solution, both single-level and dual-level calculations at the economical HF/3-21+G* level returns us more accurate results than those at the B3LYP and M06-2X levels of theory [Tables 9 and S11 (Supporting Information)].

Similarly, for the calculations of the KIE on the base-catalyzed 2′-*O*-transphosphorylation, no significant differences could be found between the single-level and dual-level results in the gas phase, as well as in the solution phase [Table S12, S13, 10, and S14 (Supporting Information)]. As shown in our previous work, by the comparison of our KIE values to the most relevant experimental KIE results, we have concluded that for the native reaction, the rate-limiting transition state is LTS, while ETS is the rate-limiting one for both S3′ and S5′ reactions.

Overall, by comparing the values of isotope effects in the gas phase with those in the solution phase, we are a little bit astonished by the fact that although the solvent effect substantially lowers the energy barriers by ~10–29 kcal/mol (Table 2), the inherent or the gas-phase isotope-effects values are fairly insensitive to the solvation environment.

In addition, remarkably, EIE and KIE values computed at the HF/3-21+G* level are at least semiquantitatively accurate, even true for single-level results. Together with all the other findings in this study about the accuracy of the HF/3-21+G* results, a solid theoretical basis is already formed toward more systematic and more accurate dual-level on-the-fly *ab initio* QM/MM free-energy and isotope effects calculations on more intricate biomolecular systems associated with the 2′-*O*-transphosphorylation.

In regard to our *ab initio* path-integral (PI) calculations of EIE and KIE using our AIF-PI method, we showed that further-quantization of only six to seven nuclei should be enough for estimating anharmonicity and tunneling effects (on top of harmonic quantization for all nuclei), in which the largest tunneling contribution is only ~0.04% (most of our other calculated values of tunneling effects are even smaller than 0.04% by at least one order of magnitude), whereas the largest anharmonic contribution is about 1% for computing $^{18}E_{Nuc}$. Therefore, we may conclude that in general anharmonicity and tunneling contributions are not particularly important to both EIE and KIE on our simplest models for the base-catalyzed 2′-*O*-transphosphorylation. Nonetheless, we should include anharmonic contribution to the EIE on the 2′-OH deprotonation. Finally, the systematic manner and the impressively fast convergence property of the powerful KP theory are also demonstrated. The largest difference in the isotope-effects calculations between first-order and second-order of KP expansions (i.e., between KP1 and KP2) is only about 0.1%, while all other differences are smaller than or in the order of magnitude of 0.01%.

## Acknowledgements

*Computing resources were partly provided by the Minnesota Supercomputing Institute, and by High Performance Cluster Computing Centre (HPCCC) and Office of Information Technology (ITO) at HKBU (sciblade and jiraiya). This work also used the Extreme Science and Engineering Discovery Environment (XSEDE).*

**Keywords:** *ab initio* · path integral · kinetic isotope effects · equilibrium isotope effects · biocatalysis · RNA · transphosphorylation · Bigeleisen equation · anharmonicity · quantum tunneling

How to cite this article: K.-Y. Wong, Y. Xu, D. M. York. *J. Comput. Chem.* **2014**, *35*, 1302–1316. DOI: 10.1002/jcc.23628

Additional Supporting Information may be found in the online version of this article.

[1] G. A. Soukup, In *Progress in Molecular Biology and Translational Science: Catalytic RNA*, Elsevier (Academic Press): Waltham, Massachusetts, **2013**, p. 232.
[2] J. K. Lassila, J. G. Zalatan, D. Herschlag, *Annu. Rev. Biochem.* **2011**, *80*, 669.
[3] F. H. Westheimer, *Science* **1987**, *235*, 1173.
[4] D. M. Perreault, E. V. Anslyn, *Angew. Chem. Int. Ed. Engl.* **1997**, *36*, 433.
[5] S. A. Strobel, J. C. Cochrane, *Curr. Opin. Chem. Biol.* **2007**, *11*, 636.
[6] M. Oivanen, S. Kuusela, H. Lönnberg, *Chem. Rev.* **1998**, *98*, 961.
[7] R. T. Raines, *Chem. Rev.* **1998**, *98*, 1045.
[8] H. Gu, S. Zhang, K.-Y. Wong, B. K. Radak, T. Dissanayake, D. L. Kellerman, Q. Dai, M. Miyagi, V. E. Anderson, D. M. York, J. A. Piccirilli, M. E. Harris, *Proc. Natl. Acad. Sci. USA.* **2013**, *110*, 13002.
[9] K.-Y. Wong, H. Gu, S. Zhang, J. A. Piccirilli, M. E. Harris, D. M. York, *Angew. Chem. Int. Ed.* **2012**, *51*, 647.
[10] K.-Y. Wong, T.-S. Lee, D. M. York, *J. Chem. Theory Comput.* **2011**, *7*, 1.
[11] T.-S. Lee, K.-Y. Wong, G. M. Giambasu, D. M. York, In Catalytic RNA; G. A. Soukup, Ed.; Elsevier (Academic Press): Waltham Massachusetts, **2013**, pp. 25.
[12] T.-S. Lee, G. M. Giambaşu, M. E. Harris, D. M. York, *J. Phys. Chem. Lett.* **2011**, *2*, 2538.
[13] B. K. Radak, M. E. Harris, D. M. York, *J. Phys. Chem. B* **2012**, *117*, 94.
[14] M. E. Harris, Q. Dai, H. Gu, D. L. Kellerman, J. A. Piccirilli, V. E. Anderson, *J. Am. Chem. Soc.* **2010**, *132*, 11613.
[15] W. G. Scott, *Curr. Opin. Struct. Biol.* **2007**, *17*, 280.
[16] F. Leclerc, *Molecules* **2010**, *15*, 5389.
[17] A. R. Ferré-D'Amaré, W. G. Scott, *Cold Spring Harb. Perspect. Biol.* **2010**, *2*, a003574.
[18] V. L. Schramm, *Chem. Rev.* **2006**, *106*, 3029.
[19] A. Kohen, H.-H. Limbach, Isotope Effects In Chemistry And Biology; Taylor & Francis: Boca Raton, **2006**.
[20] T. Strassner, *Angew. Chem. Int. Ed.* **2006**, *45*, 6420.
[21] A. C. Hengge, *Acc. Chem. Res.* **2002**, *35*, 105.
[22] K.-Y. Wong, J. P. Richard, J. Gao, *J. Am. Chem. Soc.* **2009**, *131*, 13963.
[23] K.-Y. Wong, J. Gao, *FEBS Journal* **2011**, *278*, 2579.
[24] E. L. Wu, K.-Y. Wong, X. Zhang, K. Han, J. Gao, *J. Phys. Chem. B* **2009**, *113*, 2477.
[25] K.-Y. Wong, J. Gao, *Biochemistry* **2007**, *46*, 13352.
[26] A. G. Cassano, B. Wang, D. R. Anderson, S. Previs, M. E. Harris, V. E. Anderson, *Anal. Biochem.* **2007**, *367*, 28.
[27] P. F. C. W. W. Cook, Enzyme Kinetics And Mechanism; Garland Science: London, New York, **2007**.

[28] W. W. Cleland, *Arch. Biochem. Biophys.* **2005**, *433*, 2.
[29] Y. Liu, B. A. Gregersen, A. Hengge, D. M. York, *Biochemistry* **2006**, *45*, 10043.
[30] T. Humphry, S. Iyer, O. Iranzo, J. R. Morrow, J. P. Richard, P. Paneth, A. C. Hengge, *J. Am. Chem. Soc.* **2008**, *130*, 17858.
[31] K.-Y. Wong, In Molecular Dynamics / Book 1—Theoretical Developments and Applications in Nanotechnology and Energy, L. Wang, Ed.; InTech: Rijeka, Croatia, **2012**, pp. 107.
[32] K.-Y. Wong, D. M. York, *J. Chem. Theory Comput.* **2012**, *8*, 3998.
[33] M. E. Tuckerman, Statistical Mechanics: Theory And Molecular Simulation; Oxford University Press: Oxford, New York, **2010**.
[34] B. R. Brooks, C. L. Brooks, III, A. D. Mackerell, Jr., L. Nilsson, R. J. Petrella, B. Roux, Y. Won, G. Archontis, C. Bartels, S. Boresch, A. Caflisch, L. Caves, Q. Cui, A. R. Dinner, M. Feig, S. Fischer, J. Gao, M. Hodoscek, W. Im, K. Kuczera, T. Lazaridis, J. Ma, V. Ovchinnikov, E. Paci, R. W. Pastor, C. B. Post, J. Z. Pu, M. Schaefer, B. Tidor, R. M. Venable, H. L. Woodcock, X. Wu, W. Yang, D. M. York, M. Karplus, *J. Comput. Chem.* **2009**, *30*, 1545.
[35] Y. Shao, L. F. Molnar, Y. Jung, J. Kussmann, C. Ochsenfeld, S. T. Brown, A. T. B. Gilbert, L. V. Slipchenko, S. V. Levchenko, D. P. O'Neill, R. A. DiStasio, Jr., R. C. Lochan, T. Wang, G. J. O. Beran, N. A. Besley, J. M. Herbert, C. Y. Lin, T. Van Voorhis, S. H. Chien, A. Sodt, R. P. Steele, V. A. Rassolov, P. E. Maslen, P. P. Korambath, R. D. Adamson, B. Austin, J. Baker, E. F. C. Byrd, H. Dachsel, R. J. Doerksen, A. Dreuw, B. D. Dunietz, A. D. Dutoi, T. R. Furlani, S. R. Gwaltney, A. Heyden, S. Hirata, C.-P. Hsu, G. Kedziora, R. Z. Khalliulin, P. Klunzinger, A. M. Lee, M. S. Lee, W. Liang, I. Lotan, N. Nair, B. Peters, E. I. Proynov, P. A. Pieniazek, Y. M. Rhee, J. Ritchie, E. Rosta, C. D. Sherrill, A. C. Simmonett, J. E. Subotnik, H. L. Woodcock, III, W. Zhang, A. T. Bell, A. K. Chakraborty, D. M. Chipman, F. J. Keil, A. Warshel, W. J. Hehre, H. F. Schaefer, III, J. Kong, A. I. Krylov, P. M. W. Gill, M. Head-Gordon, *Phys. Chem. Chem. Phys.* **2006**, *8*, 3172.
[36] M. Cossi, G. Scalmani, N. Rega, V. Barone, *J. Chem. Phys.* **2002**, *117*, 43.
[37] J. Khandogin, B. A. Gregersen, W. Thiel, D. M. York, *J. Phys. Chem. B* **2005**, *109*, 9799.
[38] G. Scalmani, M. J. Frisch, *J. Chem. Phys.* **2010**, *132*, 114110.
[39] D. M. York, M. Karplus, *J. Phys. Chem. A* **1999**, *103*, 11060.
[40] B. A. Gregersen, D. M. York, *J. Chem. Phys.* **2005**, *122*, 194110/1.
[41] Gaussian 09, Revision C.01, M. J. Frisch, G. W. Trucks, H. B. Schlegel, G. E. Scuseria, M. A. Robb, J. R. Cheeseman, G. Scalmani, V. Barone, B. Mennucci, G. A. Petersson, H. Nakatsuji, M. Caricato, X. Li, H. P. Hratchian, A. F. Izmaylov, J. Bloino, G. Zheng, J. L. Sonnenberg, M. Hada, M. Ehara, K. Toyota, R. Fukuda, J. Hasegawa, M. Ishida, T. Nakajima, Y. Honda, O. Kitao, H. Nakai, T. Vreven, J. A. Montgomery, Jr., J. E. Peralta, F. Ogliaro, M. Bearpark, J. J. Heyd, E. Brothers, K. N. Kudin, V. N. Staroverov, R. Kobayashi, J. Normand, K. Raghavachari, A. Rendell, J. C. Burant, S. S. Iyengar, J. Tomasi, M. Cossi, N. Rega, J. M. Millam, M. Klene, J. E. Knox, J. B. Cross, V. Bakken, C. Adamo, J. Jaramillo, R. Gomperts, R. E. Stratmann, O. Yazyev, A. J. Austin, R. Cammi, C. Pomelli, J. W. Ochterski, R. L. Martin, K. Morokuma, V. G. Zakrzewski, G. A. Voth, P. Salvador, J. J. Dannenberg, S. Dapprich, A. D. Daniels, ø. Farkas, J. B. Foresman, J. V. Ortiz, J. Cioslowski, and D. J. Fox, Gaussian, Inc., Wallingford CT, **2009**
[42] W. Kohn, *Rev. Mod. Phys.* **1999**, *71*, 1253.
[43] R. G. Parr, W. Yang, Density-Functional Theory Of Atoms And Molecules; Oxford University Press; Clarendon Press: New York NY; Oxford UK, **1989**.
[44] A. D. Becke, *J. Chem. Phys.* **1993**, *98*, 5648.
[45] J. A. Pople, *Rev. Mod. Phys.* **1999**, *71*, 1267.
[46] W. J. Hehre, L. Radom, P. v. R. Schleyer, J. A. Pople, Ab Initio Molecular Orbital Theory; Wiley: New York, **1986**.
[47] Y. Zhao, D. G. Truhlar, *Theor. Chem. Acct.* **2008**, *120*, 215.
[48] Y. Zhao, D. G. Truhlar, *Theor. Chem. Acct.* **2008**, *119*, 525.
[49] C. Møller, M. S. Plesset, *Phys. Rev.* **1934**, *46*, 618.
[50] J. A. Pople, M. Head-Gordon, K. Raghavachari, *J. Chem. Phys.* **1987**, *87*, 5968.
[51] R. O. Ramabhadran, K. Raghavachari, *J. Chem. Theory Comput.* **2013**, *9*, 3986.
[52] L. J. Schaad, L. Bytautas, K. N. Houk, *Can. J. Chem.* **1999**, *77*, 875.
[53] M. Wolfsberg, in Isotope Effects in Chemistry and Biology; A. Kohen, H.-H. Limbach, Eds.; Taylor & Francis: Boca Raton, **2006**, p. 89.
[54] K.-Y. Wong, *Commun. Comput. Phys.* **2014**, *15*, 853.
[55] K.-Y. Wong, J. Gao, *J. Chem. Phys.* **2007**, *127*, 211103.
[56] K.-Y. Wong, J. Gao, *J. Chem. Theory Comput.* **2008**, *4*, 1409.
[57] D. A. McQuarrie, Statistical Mechanics; University Science Books: Sausalito, Calif., **2000**.
[58] V. Barone, M. Cossi, J. Tomasi, *J. Chem. Phys.* **1997**, *107*, 3210.
[59] Y. Takano, K. N. Houk, *J. Chem. Theory Comput.* **2005**, *1*, 71.
[60] K.-Y. Wong, Ph.D. Thesis, Simulating Biochemical Physics with Computers: 1. Enzyme Catalysis by Phosphotriesterase and Phosphodiesterase; 2. Integration-Free Path-Integral Method for Quantum-Statistical Calculations, University of Minnesota: Minneapolis, **2008**.
[61] H. Kleinert, *Path Integrals In Quantum Mechanics, Statistics, Polymer Physics, And Financial Markets*, 5th ed.; World Scientific Singapore; Hackensack, NJ, **2009**.
[62] R. P. Feynman, A. R. Hibbs, D. F. Styer, Quantum Mechanics And Path Integrals, Emended ed.; Dover Publications: Mineola, NY, **2005**.
[63] M. J. Gillan, *Phys. Rev. Lett.* **1987**, *58*, 563.
[64] M. J. Gillan, *J. Phys. C: Solid State Phys.* **1987**, *20*, 3621.
[65] G. A. Voth, *J. Phys. Chem.* **1993**, *97*, 8365.
[66] J. Cao, G. A. Voth, *J. Chem. Phys.* **1994**, *101*, 6168.
[67] G. A. Voth, *Adv. Chem. Phys.* **1996**, *93*, 135.
[68] (a) R. Ramírez, T. López-Ciudad, J. C. Noya, *Phys. Rev. Lett.* **1998**, *81*, 3303; (b) Comment: Andronico, G.; Branchina, V.; Zappala, D. *Phys. Rev. Lett.* **2002**, *88*, 178901; (c) Reply to comment: Ramirez, R.; López-Ciudad, T. *Phys. Rev. Lett.* **2002**, *88*, 178902.
[69] R. Ramírez, T. López-Ciudad, *J. Chem. Phys.* **1999**, *111*, 3339.
[70] G. A. Voth, D. Chandler, W. H. Miller, *J. Chem. Phys.* **1989**, *91*, 7749.
[71] S. Jang, C. D. Schwieters, G. A. Voth, *J. Phys. Chem. A* **1999**, *103*, 9527.
[72] (a) S. Jang, G. A. Voth, *J. Chem. Phys.* **2000**, *112*, 8747; (b) *Erratum*: **2001**, *114*, 1944.
[73] J. Gao, D. T. Major, Y. Fan, Y.-l. Lin, S. Ma, K.-Y. Wong, in Molecular Modeling of Proteins; A. Kukol, Ed.; Humana Press: Totowa, NJ, **2008**, pp. 37.
[74] D. T. Major, A. Heroux, A. M. Orville, M. P. Valley, P. F. Fitzpatrick, J. Gao, *Proc. Natl. Acad. Sci. USA* **2009**, *106*, 20734.
[75] A. Warshel, M. H. M. Olsson, J. Villa-Freixa, in Isotope Effects in Chemistry and Biology; A. Kohen, H.-H. Limbach, Eds.; Taylor & Francis: Boca Raton, **2006**, pp. 621.
[76] J. Gao, K.-Y. Wong, D. T. Major, *J. Comput. Chem.* **2008**, *29*, 514.
[77] M. Wang, Z. Lu, W. Yang, *J. Chem. Phys.* **2006**, *124*, 124516.
[78] Q. Wang, S. Hammes-Schiffer, *J. Chem. Phys.* **2006**, *125*, 184102.
[79] D. T. Major, J. Gao, *J. Am. Chem. Soc.* **2006**, *128*, 16345.
[80] N. Chakrabarti, T. Carrington, Jr., B. Roux, *Chem. Phys. Lett.* **1998**, *293*, 209.
[81] M. J. Field, M. Albe, C. Bret, F. P.-D. Martin, A. Thomas, *J. Comput. Chem.* **2000**, *21*, 1088.
[82] H. Kleinert, *Phys. Lett. A* **1993**, *173*, 332.
[83] J. Jaenicke, H. Kleinert, *Phys. Lett. A* **1993**, *176*, 409.
[84] H. Kleinert, H. Meyer, *Phys. Lett. A* **1994**, *184*, 319.
[85] H. Kleinert, W. Kürzinger, A. Pelster, *J. Phys. A: Math. Gen.* **1998**, *31*, 8307.
[86] M. Bachmann, H. Kleinert, A. Pelster, *Phys. Rev. A* **1999**, *60*, 3429.
[87] W. Janke, A. Pelster, H.-J. Schmidt, M. Bachmann, Fluctuating Paths And Fields : Festschrift Dedicated To Hagen Kleinert On The Occasion Of His 60th Birthday; World Scientific: River Edge, NJ, **2001**.
[88] S. L. Mielke, D. G. Truhlar, *J. Chem. Theory Comput.* **2012**, *8*, 1589.
[89] Mathematica. Wolfram Research, Inc., Mathematica, Versions 5, 6, and 9; Wolfram Research, Inc.: Champaign, IL, **2012**.
[90] X. Liu, C. B. Reese, *Tetrahedron Lett.* **1995**, *36*, 3413.
[91] X. Liu, C. B. Reese, *Tetrahedron Lett.* **1996**, *37*, 925.
[92] X. Liu, C. B. Reese, *J. Chem. Soc. Perkin. Trans. 1* **2000**, 2227.
[93] S. Iyer, A. C. Hengge, *J. Org. Chem.* **2008**, *73*, 4819.
[94] J. B. Thomson, B. K. Patel, V. Jimenez, K. Eckart, F. Eckstein, *J. Org. Chem.* **1996**, *61*, 6273.
[95] L. B. Weinstein, D. J. Earnshaw, R. Cosstick, T. R. Cech, *J. Am. Chem. Soc.* **1996**, *118*, 10341.
[96] C. L. Dantzman, L. L. Kiessling, *J. Am. Chem. Soc.* **1996**, *118*, 11715.

Received: 10 March 2014
Accepted: 6 April 2014
Published online on 20 May 2014